Composite Structures 304 (2023) 116322

Contents lists available at ScienceDirect

Composite Structures

journal homepage: www.elsevier.com/locate/compstruct

Multi-objective topology optimization filled with multiple microstructures

Wenjun Chen, Yongfeng Zheng, Yingjun Wang *

National Engineering Research Center of Novel Equipment for Polymer Processing, The Key Laboratory of Polymer Processing Engineering of the Ministry of Education, Guangdong Provincial Key Laboratory of Technique and Equipment for Macromolecular Advanced Manufacturing, South China University of Technology, Guangzhou 510641, China

ARTICLE INFO

Keywords:
Multi-objective topology optimization
Steady-state heat conduction
Eigenvalue optimization
Multiple microstructures
Lattice material

ABSTRACT

Structures in engineering application may face loads from multiple physical fields. To simultaneously design macroscopic structures that have lower thermal compliance and higher natural frequency, a new multi-objective topology optimization filled with multiple microstructures is proposed based on the weight sum method. To shorten the gap between the optimized results and the design requirement, a self-selected weight sum method that is based on the fitting functions of the result domains and the bisection method is proposed to get the optimized macroscopic structures with specific properties directly. Several numerical examples, including single-phase material and multiple materials cases, are presented to demonstrate the feasibility and practicality of the proposed method. The results show that the employment of multiple materials optimization provides the structures with a wider result domain than the single-phase material situations. The self-selected weight sum method is of high efficiency, good connectivity and easy to implement.

1. Introduction

Topology optimization (TO) is a structural design method aiming at finding out the optimal material distribution subjected to some constrains within a given design domain. Since the pioneering work of Bendsøe and Kikuchi [1], plenty of impressive TO methods have arisen in the past few decades, such as homogenization method [1], solid isotropic material with penalization (SIMP) approach [2], evolutionary structural optimization (ESO) [3], level set method (LSM) [4,5], and moving morphable component (MMC) method [6,7]. Among above-mentioned methods, the SIMP method has been widely used due to its simplicity [8]. Hence, it will be used in this study to establish the multi-objective optimization model. Additionally, TO has been successfully applied to various physical fields such as solid mechanics [9], fluid mechanics [10], heat transfer [11,12], and engineering fields like aircraft and additive manufacturing [13,14].

The steady-state heat conductive TO can be regarded as an important application of TO in thermal conductive problem. Plenty of earlier steady-state heat conductive works focus on the calculation of shape-based sensitivities, which cover aspects in steady-state and transient fields with respect to the changes in design parameters [15], sensitivities for heat conducting solids [16], sensitivities for linear [17] and non-linear [18] thermal systems. Since TO can provide a more flexible design comparing with the size or the shape optimization, designers began to introduce TO into thermal problems [19]. Li et al [20] presented a procedure for both shape and topology optimizations for heat conductive problems. Soon after that, Bendsøe and Sigmund [21] put forward a classical work that obtains a 'tree-like' structure based on a two-dimensional (2-D) finite element framework. Gersbory-Hansen et al. [22] adopted the finite volume method in conjunction with TO to solve a similar planar heat conduction problem, and a similar branching characteristic is obtained. Zhuang et al. [23] combined the level set method with topological derivatives to solve the planar heat conduction problem. Li et al. [19] adopted evolutionary algorithms in 2D topology design of heat conduction problem, which was extended to three-dimensional (3-D) design latter [24–26]. The efficiency and accuracy of the steady-state heat conductive TO are gradually attracting attention nowadays, which are heavily dependent on the initial design, analysis mesh and filtering methods [27,28]. To get rid of the influence of analysis mesh, Zhao et al. [29] presented a novel meshless TO method that based on the meshless generalized finite difference method, and it has better performance in feasibility and stability. Lohan et al. [30] proposed a more comprehensive approach by combining steady-state thermal TO with a generation algorithm, which is independent of the initial material distribution and mesh, and does not require a filter. Among the methods above, the classical optimization model proposed

* Corresponding author.
E-mail address: wangyj84@scut.edu.cn (Y. Wang).

https://doi.org/10.1016/j.compstruct.2022.116322
Received 9 March 2022; Received in revised form 14 July 2022; Accepted 7 October 2022
Available online 14 October 2022

by Bendsøe and Sigmund [21] has been widely used for its simplicity. In this paper, it will be used to establish the multi-objective optimization model.

Besides, eigenvalue optimization is also of great importance in many engineering fields. It is expected to heighten the structural natural frequencies to avoid destructive responses caused by external excitations. It contains TO problems related to the fundamental frequency, the high-order frequency, and the frequency gap of a number of the lower frequencies [31]. This paper mainly addresses the TO for maximizing the first fundamental frequency. Díaz and Kikuchi [32] firstly combined the TO of the continuum structure with the natural frequency optimization of structural vibration, where they used the homogenization method to address the single frequency design of plane disks. Soon after that, Tenek and Hagiwara [33] proposed an enhanced form of optimization model based on the homogenization or the SIMP method. Ma et al. [34,35] defined a different objective function for maximizing the fundamental frequency, and both the repeated eigenvalue optimization problems and the frequency response of structural TO problem were discussed in their studies. Pedersen [36] proposed a TO models using the SIMP approach for maximizing the first natural frequency, which mainly focused on removing localized modes in low density areas of the design domain. Du and Olhoff [37] studied the fundamental frequency, high-order natural frequency and frequency gap optimization design using the SIMP method. Achtziger and Kocvara [38] developed a non-heuristic mathematical models using an equivalent reformulation as a bilinear semi-definite programming problem without the pitfalls of the origin problem to improve the situation where some design variables were equal to zero. Liu et al. [31] presented a frequency optimization method based on the compactly supported radial basis functions parameterized level-set method, which adopts the fundamental frequency, the frequency of a given higher-order, and the gap between two consecutive frequencies as the optimization objectives. More recently, Ferrari et al. [39] proposed an eigenvalue TO method that surrogated the eigenvalue problem by a frequency response one, and it got a remarkable improvement in the calculation cost.

Multi-objective topology optimization is characterized by the ability to simultaneously design several different properties of the structures. In a recent work, Pereira et al. [40] presented a method aiming at maximizing the fundamental model frequency and corresponding specific damping capacity of tow-steered composite laminates, in which the theoretical derivation of the multi-objective TO and data analysis of a series of numerical examples are made clearly. In this paper, the multi-objective function is defined to obtain macrostructures with lower thermal compliance and higher natural frequency. However, due to the performance conflicts between low thermal compliance and high natural frequency, it can be known that any further improvement in one objective will result in a clear weakening of the other [41]. Pareto optimum is thus defined, where there is no solution that an objective is optimized without deteriorating the other one. In general, it is hard to generate a global optimum for all the anticipated objectives. This paper focuses on the relation between different objective functions. The weight sum method is used to depict the Pareto optimal set, where multiple solution points can be obtained by varying the weights consistently [42]. The interaction between different objectives can be obtained by analyzing the solution points.

To perform better in both the heat conduction and natural frequency, the macrostructures can be filled by multiple microstructure. In the process of multiple material Topology optimization (MMTO), the material interpolation scheme is usually needed to obtain the effective mechanical properties of an element. Bendsøe and Sigmund [21] firstly proposed a modified SIMP method to construct the material interpolation model, which is widely applied in MMTO [43,44]. Following this work, researchers proposed some other methods like SIMP. Blasques [45] proposed a SIMP-like material interpolation method in the TO of laminated composite beam cross sections. Zuo and Saitou [8] presented an ordered multi-materials SIMP interpolation to solve MMTO problems without introducing any new variables. Besides, other researchers tried to use the other algorithm to deal with the material interpolation problem. Habibian et al. [46] proposed an approach for solving density-based MMTO of cracked structures using Peridynamics. Gao et al. [47] proposed an method for robust MMTO problem of continuum structures under load uncertainly. Banh et al. [48] came up with a non-homogeneous MMTO method for functionally graded structures with cracks, which used the active-phase algorithm to convert a MMTO problem into many binary phase TO sub-problems. The above three methods are based on alternating active-phase method, and both of them effectively solve the problem. Li et al. [49] presented a MMTO method that assigned the material according to the material utilization based on the BESO. In terms of the difference of filling materials, Giraldo-Londono and Paulino [50] proposed a MMTO method filling by multiple viscoelastic microstructures based on the Discrete Material Optimization interpolation scheme. Due to the convenience and generality, the modified SIMP method proposed is used in this paper.

This paper proposes a novel multi-objective TO method, where the maximization of natural frequency and the minimization of thermal compliance are considered simultaneously. To enhance the performance of the structures from the aspect of microstructure, multiple lattice materials are used to constitute the macrostructure. The lattices selected have high performance in both the heat conduction and mechanics. The energy-based homogenization method (EBHM) is used to calculate the effective property of lattice materials, and the modified SIMP method is employed as the material interpolation scheme.

Comparing with the previous work, this paper pays more attention in the result of the multi-objective optimization under different material proportions. Optimized structures with different properties can be obtained by adjusting the material proportion. Based on this fact, a self-selected weight sum method is proposed in this paper, which can approach and obtain the target result point by adjusting the filling proportion. This method can effectively expand the result domain of multi-objective topology optimization, and obtain the target result points directly, which can remarkably shorten the design time.

The remainder of this paper is organized as follows: Section 2 shows the EBHM and the material interpolation method. The effective elastic properties of lattices will also be calculated used the EBHM in section 2. The establishment of the optimization model will be conducted in Section 3. The Optimality Criteria (OC) method and the analysis of sensitivity are introduced briefly in Section 4. Section 5 provides several numerical examples to show the feasibility and the advantage of the multi-objective TO method. Finally, conclusions are given in Section 6.

2. Theory background

2.1. Homogenization theory

The homogenization theory can be applied to evaluate material effective properties, when satisfying the following two assumptions: (1) the dimensional sizes of the periodic unit cells (PUCs) are much smaller than that of the macrostructures, and (2) PUCs are periodically distributed in the macrostructure [51,52]. Since it was proposed, homogenization methods have played a significant role in calculating the elastic properties of microstructures [53,54] and viscoelastic materials [50]. Among the existing homogenization methods with different characteristics, numerical homogenization method [55] and the EBHM [56] attracted the most attention. The latter one is based on the criterion of energy conservation with respect to stress and strain. In this paper, EBHM is adopted to evaluate the macroscopic equivalent properties of microstructures for convenience.

In this case, the asymptotic expansion theory is used in characterizing the displacement field inside PUCs [52], which can be expressed as.

$$u^t(a,b) = u_0(a,b) + tu_1(a,b) + t^2u_2(a,b) + \cdots \quad (1)$$

Table 1
Microstructures and their mechanical properties.

Microstructure	Area	Elastic matrix	Thermal elastic matrix
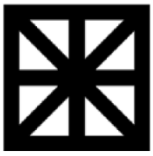	0.3	$1.0\times10^6\times\begin{bmatrix}3.1197 & 0.7046 & 0.0000\\ 0.7046 & 3.1197 & 0.0000\\ 0.0000 & 0.0000 & 0.6132\end{bmatrix}$	$\begin{bmatrix}0.1817 & 0.0000\\ 0.0000 & 0.1817\end{bmatrix}$
	0.5	$1.0\times10^6\times\begin{bmatrix}5.6803 & 1.4037 & 0.0000\\ 1.4037 & 5.6803 & 0.0000\\ 0.0000 & 0.0000 & 1.2444\end{bmatrix}$	$\begin{bmatrix}0.3251 & 0.0000\\ 0.0000 & 0.3251\end{bmatrix}$
	0.7	$1.0\times10^6\times\begin{bmatrix}9.2344 & 2.4706 & 0.0000\\ 2.4706 & 9.2344 & 0.0000\\ 0.0000 & 0.0000 & 2.4932\end{bmatrix}$	$\begin{bmatrix}0.5118 & 0.0000\\ 0.0000 & 0.5118\end{bmatrix}$
	0.3	$1.0\times10^6\times\begin{bmatrix}2.7960 & 0.7777 & 0.0000\\ 0.7777 & 2.7960 & 0.0000\\ 0.0000 & 0.0000 & 0.7109\end{bmatrix}$	$\begin{bmatrix}0.1704 & 0.0000\\ 0.0000 & 0.1704\end{bmatrix}$
	0.5	$1.0\times10^6\times\begin{bmatrix}5.3898 & 1.6396 & 0.0000\\ 1.6396 & 5.3898 & 0.0000\\ 0.0000 & 0.0000 & 1.5501\end{bmatrix}$	$\begin{bmatrix}0.3230 & 0.0000\\ 0.0000 & 0.3230\end{bmatrix}$
	0.7	$1.0\times10^6\times\begin{bmatrix}8.6149 & 2.6471 & 0.0000\\ 2.6471 & 8.6149 & 0.0000\\ 0.0000 & 0.0000 & 2.7868\end{bmatrix}$	$\begin{bmatrix}0.4956 & 0.0000\\ 0.0000 & 0.4956\end{bmatrix}$

where the involved functions are dependent on the global macroscopic variable a and the local microscopic variable b. $t=b/a$ is the scale factor, it is easy to find that PUCs will approach to be a point when $t\approx 0$. When only considering the first order terms of the displacement field $u^t(a,b)$, the homogenized effective elastic tensor E^H of the microstructures can be obtained by the volume integrant in PUCs:

$$E^H_{ijkl}=\frac{1}{|\mathrm{Y}|}\int_Y E_{pqrs}(\varepsilon^{0(kl)}_{pq}-\varepsilon^{*(kl)}_{pq})(\varepsilon^{0(kl)}_{rs}-\varepsilon^{*(kl)}_{rs})dY \tag{2}$$

where $|\mathrm{Y}|$ denotes the area in 2D cases and the volume in 3D cases of PUCs, $\varepsilon^{0(ij)}_{pq}$ corresponds to three linearly independent unit test strain fields in the 2D scenario, namely $(1,0,0)^T$, $(0,1,0)^T$ and $(0,0,1)^T$. The unknown item $\varepsilon^{*(kl)}_{pq}$ is the Y-periodic solution of the following equilibrium equation.

$$\int_Y E_{ijpq}\varepsilon^{*(kl)}_{rs}\frac{\partial\varpi_i}{\partial y_j}dY=\int_Y E_{ijpq}\varepsilon^{0(kl)}_{rs}\frac{\partial\varpi_i}{\partial y_j}dY \tag{3}$$

where ϖ is the admissible displacement field.

If the considered PUC is divided into N_e elements, the homogenized elastic property showed in Eq. (2) can be approximated by:

$$E^H_{ijkl}=\frac{1}{|\mathrm{Y}|}\sum_{e=1}^{N_e}(\boldsymbol{u}^{0(ij)}_e-\boldsymbol{u}^{*(ij)}_e)^T\boldsymbol{k}_e(\boldsymbol{u}^{0(kl)}_e-\boldsymbol{u}^{*(kl)}_e) \tag{4}$$

where $\boldsymbol{u}^{*(ij)}_e$ is unknown element displacements, and $\boldsymbol{k}_e$ is the element stiffness matrix.

In the EBHM, the unit test strains are imposed directly on the boundaries of the PUCs. The induced strain field $\varepsilon^{A(kl)}_{pq}$ corresponds to the superimposed strain fields $(\varepsilon^{0(kl)}_{pq}-\varepsilon^{*(kl)}_{pq})$ in Eq. (2) [56]. In terms of element mutual energies, (4) is written in a new equivalent form as [57]:

$$E^H_{ijkl}=\frac{1}{|\mathrm{Y}|}\sum_{e=1}^{N_e}Q^e_{ijkl}=\frac{1}{|\mathrm{Y}|}\sum_{e=1}^{N_e}(\boldsymbol{u}^{\Lambda(ij)}_e)^T\boldsymbol{k}_e(\boldsymbol{u}^{\Lambda(kl)}_e) \tag{5}$$

where $\boldsymbol{u}^{A(ij)}_e$ denotes the corresponding element displacements, and Q^e_{ijkl} represents the element mutual energy. The effective elasticity properties are interpreted as the summation of elastic energies of PUCs [19,57]. In 2D cases, the homogenized elastic tensor E^H is expanded as:

$$E^H=\begin{bmatrix}E^H_{1111} & E^H_{1122} & E^H_{1112}\\ E^H_{2211} & E^H_{2222} & E^H_{2212}\\ E^H_{1211} & E^H_{1222} & E^H_{1212}\end{bmatrix} \tag{6}$$

The thermal elastic tensor can also be obtained by applying the method above. The difference in calculating the thermal elastic tensor is that two unit test temperature gradients will be imposed directly on the boundaries of the PUCs, which are $(1,0)^T$ and $(0,1)^T$, respectively. And the homogenized thermal elastic tensor E^{H-ther} can be expanded as:

$$E^{H-ther}=\begin{bmatrix}E^{H-ther}_{1111} & E^{H-ther}_{1122}\\ E^{H-ther}_{2211} & E^{H-ther}_{2222}\end{bmatrix} \tag{7}$$

2.2. Calculation of the equivalent elastic properties

Lattice materials are used in this paper, whose properties can be designed by changing the geometrical configurations. The mechanical properties of a lattice are mainly dependent on the topology of the unit cell, whose characteristic length should be at least one order of magnitude below that of the component, and should be periodic so that a lattice can be considered as a material.

Two lattice materials are selected and the EBHM is used to calculate their mechanical properties. Herein, since lattice materials will be used for both the natural frequency optimization and thermal conductivity optimization, the elastic matrix and thermal elastic matrix of lattice materials should be calculated. Assuming all the PUCs used in this section are first order square unit, and the elasticity modulus of the base material E_0 is equal to 2×10^7 Pa, which can reduce the size difference between the values of the objective functions, while the heat conductive capacity E^h_0 of the base material and the Poisson ratio *nu* are equal to 1 W/(m*K) and 0.3, respectively. Applying the above parameters to the EBHM, elastic matrix and thermal elastic matrix can be obtained. The lay-out and mechanical properties can be seen in Table 1.

For convenience, the first and second microstructures are named as material α and material β respectively.

2.3. Material interpolation scheme

In this paper, multiple microstructures are used to fill the macroscopic structure. The material interpolation scheme is required to figure out the effective mechanical properties.

The SIMP formulation is applied here, which was first extended to the multiple materials case by Bendsøe and Sigmund [58]. According to the SIMP interpolation model, the effective mechanical properties of a single element with three phases (including two kinds of solid materials and one void material) of materials can be expressed as:

$$E_e(x_{ij},y_{ij})=(x_{ij})^P\left\{(y_{ij})^PE^2_0+\left[1-(y_{ij})^P\right]E^1_0\right\} \tag{8}$$

where E^1_0 and E^2_0 indicate the elastic modulus of material-1 and material-

Table 2
Situation of different materials distribution.

Situation Number	x_{ij}	y_{ij}	Material contains
1	0	0	No material
2	1	0	Full of material 1
3	1	1	Full of material 2
4	1	(0,1)	Material 1 and 2

2 respectively. When the element contains solid materials (x_{ij} is higher than 0), y_{ij} represents the contribution of solid material-1 and solid material-2 to the effective elastic modulus of element e. Besides, P is the penalization exponent that can help promote convergence to a discrete solution by lowering the local stiffness of the element with intermediate density. To better illustrate material contribution in the element when the variables x_{ij} and y_{ij} change, Table 2 is proposed here.

3. Problem statement

This section establishes a multi-objective optimization model, which involves two performances in both the heat conduction and natural frequency. The weighted-sum method is used to formulate the multi-objective optimization model as:

$$\begin{aligned}
\text{Find} \quad & : \quad x = [x_1, x_2, x_3, \ldots, x_n], \\
& \quad\; y = [y_1, y_2, y_3, \ldots, y_n] \\
\textit{Minimize} \quad & : \quad F = (1-\psi)C - \psi{\omega_1}^2 \\
\textit{Subject to} \quad & : \quad \boldsymbol{K}^h\boldsymbol{T} = \boldsymbol{f}, \\
& \quad\; [\boldsymbol{K} - {\omega_1}^2\boldsymbol{M}]\boldsymbol{u}_1 = 0, \\
& \quad\; V_{xmax} - \sum_{i=1}^{n} V_i x_i = 0, \\
& \quad\; V_{ymax} - \sum_{i=1}^{n} V_i y_i = 0, \\
& \quad\; 0 \le x_{min} \le x_i \le x_{max} \le 1, \\
& \quad\; 0 \le y_{min} \le y_i \le y_{max} \le 1, \\
& \quad\; 0 \le \psi \le 1
\end{aligned} \tag{9}$$

where $\boldsymbol{f}$ is the thermal load vector, $\boldsymbol{T}$ is the temperature vector, $\boldsymbol{K}^h$ is the thermal conductivity in at the macro level, $\boldsymbol{K}$ is the stiffness matrix of elastic problem, $\boldsymbol{M}$ is the global mass matrix, ω_1 is the first natural frequency of vibrating continuum structures, respectively. Besides, V_{xmax} and V_{ymax} are the prescribed structural volume of variables x and y respectively, V_i is the volume of the i-th element. x_i is the density of the i-th element, y_i represents the contribution of different materials, n is the total number of elements. $x_{\min}$ and $y_{\min}$ is the lower limit of x_i and y_i, while $x_{\max}$ and $y_{\max}$ is the upper limit of x_i and y_i. To avoid the computational singularities, $x_{\min}$ is equal to 0.001. Since the multi-objective function defined in Eq. (9) only focuses on two properties of the continuum structures, a simple weighted-sum method has been applied, where ψ is the weight coefficient. The thermal compliance C can be expressed as

$$C = \boldsymbol{T}^T\boldsymbol{K}^h\boldsymbol{T} = \sum_{i=1}^{N} \boldsymbol{T}_e^T\boldsymbol{K}_e^h\boldsymbol{T}_e \tag{10}$$

where $\boldsymbol{T}_e$ and ${\boldsymbol{K}_e}^h$ are the temperature vector and the elemental heat conductivity matrix respectively. In the same way, $\omega_1^2(\mathrm{x})$ is the objective of natural frequency optimization problem, which is the square of the first natural frequency, and it can be expressed as

$$\omega_1^2 = \frac{\boldsymbol{u}^T\boldsymbol{K}\boldsymbol{u}}{\boldsymbol{u}^T\boldsymbol{M}\boldsymbol{u}} \tag{11}$$

where $\boldsymbol{u}$ is the eigenvector corresponding to ω_1.

The global mass matrix $\boldsymbol{M}$ is assembled by the element mass matrix $\boldsymbol{M}_e$, which is the combination of consistent mass matrix and lumped mass matrix. It can be written as

$$\boldsymbol{M}_e = \beta\boldsymbol{M}_e^c + (1-\beta)\boldsymbol{M}_e^l \tag{12}$$

where β is the binding coefficient, which is equal to 0.5 in this paper, $\boldsymbol{M}_e^c$ and $\boldsymbol{M}_e^l$ are the consistent mass matrix and lumped mass matrix respectively, and the formulas can be expressed by:

$$\boldsymbol{M}_e^c = x\int_v N^T N dv \tag{13}$$

$$\boldsymbol{M}_e^l = \frac{1}{4}xAI_{(8\times 8)} \tag{14}$$

where N is the shape function of the Q-4 element, A is the area of one element, and $I_{(8\times 8)}$ is the identity matrix. Obviously, all the elements are the same in size. The element mass matrix is only dependent on the variable x.

4. Sensitivity analysis and algorithm implementation

Since the objective function of Eq. (9) is consisted of two different TO problems, and both of them are depended on variables x_{ij} and y_{ij} instead of the weight ψ, in this section, the objective function of multi-objective TO will be separated into two parts (steady-state heat conductivity optimization and natural frequency optimization) to analyze the sensitivity respectively. And then it will be put together to get the sensitivity of the multi-objective problem.

Firstly, for both of two different objective functions, stiffness matrix is defined before sensitivity analysis. According to the finite element analysis, the element stiffness matrix can be obtained through the following formula

$$\boldsymbol{K}_e = \int_v \boldsymbol{B}\boldsymbol{D}_e\boldsymbol{B}dv \tag{15}$$

where $\boldsymbol{B}$ is the strain–displacement matrix. Referring to Eq. (8), the effective elastic matrix and effective thermal elastic matrix of the element containing multiple microstructures can be expressed as.

$$\boldsymbol{D}_e(x_i, y_i) = (x_i)^P\left\{(y_i)^P\boldsymbol{D}_0^2 + \left[1-(y_i)^P\right]\boldsymbol{D}_0^1\right\} \tag{16}$$

where $\boldsymbol{D}_e$ indicates the effective elastic matrix of element-i, $\boldsymbol{D}_0^1$ and $\boldsymbol{D}_0^2$ are the elastic matrixes of the microstructure-1 and microstructure-2 used to fill in the element. The element stiffness matrix can be acquired by combining Eq. (15) with Eq. (16).

Secondly, the sensitivity of heat conductive TO is analyzed. Its objective function can be found in Eq. (10) of section 3. When using the multiple materials interpolation scheme, the elemental heat conductivity matrix depends on variables x_{ij} and y_{ij}. According to the chain rule and the adjoint method [21], the derivative of the thermal compliance with respect to variables x_{ij} and y_{ij} can be written as

$$\begin{aligned}
\frac{\partial C}{\partial x_i} &= -\boldsymbol{T}_e^T\frac{\partial \boldsymbol{K}_e^h}{\partial x_i}\boldsymbol{T}_e \\
&= -\boldsymbol{T}_e^T\cdot\int_v \boldsymbol{B}^h\frac{\partial \boldsymbol{D}_e^h}{\partial x_i}\boldsymbol{B}^h dv\cdot\boldsymbol{T}_e \\
&= -\boldsymbol{T}_e^T\cdot\int_v \boldsymbol{B}^h P\cdot x_i^{P-1}\left\{y_i^P D_0^2 + \left[1-(y_i)^P\right]D_0^1\right\}\boldsymbol{B}^h dv\cdot\boldsymbol{T}_e \\
&= -\boldsymbol{T}_e^T\cdot x_i^{-1}\cdot\int_v \boldsymbol{B}^h P\cdot x_i^P\left\{y_i^P D_0^2 + \left[1-(y_i)^P\right]D_0^1\right\}\boldsymbol{B}^h dv\cdot\boldsymbol{T}_e
\end{aligned} \tag{17}$$

Combining with Eq. (16), Eq. (17) can be rewritten as:

$$\frac{\partial C}{\partial x_i} = -\boldsymbol{T}_e^T\frac{\partial \boldsymbol{K}_e^h}{\partial x_i}\boldsymbol{T}_e = -P\cdot x_i^{-1}\cdot\boldsymbol{T}_e^T\cdot\boldsymbol{K}_e^h\cdot\boldsymbol{T}_e \tag{18}$$

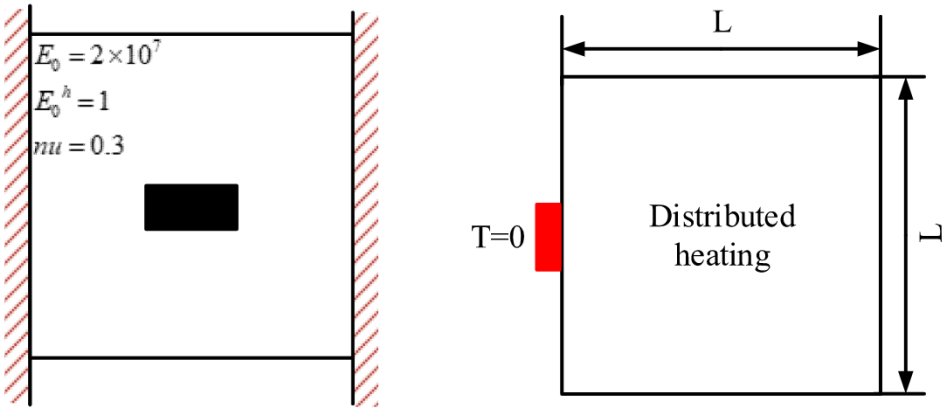

Fig. 1. Loads and boundary conditions for Example 1.

$$\begin{aligned}\frac{\partial C}{\partial y_i} &= -\boldsymbol{T}_e^T\frac{\partial \boldsymbol{K}_e^h}{\partial y_i}\boldsymbol{T}_e \\ &= -\boldsymbol{T}_e^T\cdot\int_v \boldsymbol{B}^h\frac{\partial \boldsymbol{D}_e^h}{\partial y_i}\boldsymbol{B}^h dv\cdot\boldsymbol{T}_e \\ &= -P\cdot x_i^P\cdot y_i^{P-1}\cdot\boldsymbol{T}_e^T\cdot\left(\boldsymbol{K}_2^h-\boldsymbol{K}_1^h\right)\cdot\boldsymbol{T}_e\end{aligned} \tag{19}$$

where $\boldsymbol{D}_e^h$ indicates the effective thermal elastic matrix of the i-th element, $\boldsymbol{B}^h$ is the strain–displacement matrix in heat conductive optimization. $\boldsymbol{K}_2^h$ and $\boldsymbol{K}_1^h$ can be obtained through the expressions:

$$\boldsymbol{K}_1^h = \int_v \boldsymbol{B}^h\boldsymbol{D}_0^{h1}\boldsymbol{B}^h dv \tag{20}$$

$$\boldsymbol{K}_2^h = \int_v \boldsymbol{B}^h\boldsymbol{D}_0^{h2}\boldsymbol{B}^h dv \tag{21}$$

where $\boldsymbol{D}_0^{h1}$ and $\boldsymbol{D}_0^{h2}$ are the thermal elastic matrixes of microstructure-1 and microstructure-2, respectively.

Thirdly, according to Eq. (11), the first derivation of the eigenvalue TO objective function with respect to variable x_{ij} can be expressed as

$$\begin{aligned}\frac{\partial \omega_1^2}{\partial x_i} &= -\frac{\boldsymbol{u}_i^T\frac{\partial \boldsymbol{K}_e}{\partial x_i}\boldsymbol{u}_i\boldsymbol{u}_i^T\boldsymbol{M}_e\boldsymbol{u}_i-\boldsymbol{u}_i^T\boldsymbol{K}_e\boldsymbol{u}_i\boldsymbol{u}_i^T\frac{\partial \boldsymbol{M}_e}{\partial x_i}\boldsymbol{u}_i}{\left(\boldsymbol{u}_i^T\boldsymbol{M}_e\boldsymbol{u}_i\right)^2} \\ &= -\frac{\boldsymbol{u}_i^T\left(\int_v \boldsymbol{B}\frac{\partial \boldsymbol{D}_e}{\partial x_i}\boldsymbol{B}dv-\omega_1^2\frac{\partial \boldsymbol{M}_e}{\partial x_i}\right)\boldsymbol{u}_i}{\boldsymbol{u}_i^T\boldsymbol{M}_e\boldsymbol{u}_i} \\ &= -\frac{\boldsymbol{u}_i^T\cdot P\cdot\left(x_i^{-1}\cdot\boldsymbol{K}_e-\omega_1^2\cdot x_i^{P-1}\cdot\boldsymbol{M}_e\right)\cdot\boldsymbol{u}_i}{\boldsymbol{u}_i^T\boldsymbol{M}_e\boldsymbol{u}_i}\end{aligned} \tag{22}$$

Known from Section 3.1, the element mass matrix is independent of the material distribution in a certain element, which is determined by the variable y_{ij}. Consequently, the first derivation of ω_1^2 with respect to the variable y_{ij} can be expressed as:

$$\begin{aligned}\frac{\partial \omega_1^2}{\partial y_i} &= -\frac{\boldsymbol{u}_i^T\frac{\partial \boldsymbol{K}_e}{\partial y_i}\boldsymbol{u}_i}{\boldsymbol{u}_i^T\boldsymbol{M}_e\boldsymbol{u}_i} \\ &= -\frac{P\cdot x_i^P\cdot y_i^{P-1}\cdot\boldsymbol{u}_i^T\cdot\left(\boldsymbol{K}_2-\boldsymbol{K}_1\right)\cdot\boldsymbol{u}_i}{\boldsymbol{u}_i^T\boldsymbol{M}_e\boldsymbol{u}_i}\end{aligned} \tag{23}$$

where $\boldsymbol{K}_1$ and $\boldsymbol{K}_2$ can be obtained through the following formulas:

$$\boldsymbol{K}_1 = \int_v \boldsymbol{B}\,\boldsymbol{D}_0^1\boldsymbol{B}\,dv \tag{24}$$

$$\boldsymbol{K}_2 = \int_v \boldsymbol{B}\,\boldsymbol{D}_0^2\boldsymbol{B}\,dv \tag{25}$$

Finally, combining the sensitivity of heat conduction and natural frequency, the sensitivity of the multi-objective function can be directly derived as.

$$\frac{\partial F}{\partial x_i} = (1-\psi)\frac{\partial C}{\partial x_i}-\psi\frac{\partial \omega_1^2}{\partial x_i} \tag{26}$$

$$\frac{\partial F}{\partial y_i} = (1-\psi)\frac{\partial C}{\partial y_i}-\psi\frac{\partial \omega_1^2}{\partial y_i} \tag{27}$$

The optimization problem can be solved using several different methods such as Optimality Criteria (OC) method, Sequential Linear Programming (SLP) methods, the Method of Moving Asymptotes (MMA), etc. Among them, OC method is widely used for its simplicity. To reduce the computation time, this paper adopts the OC method. A heuristic updating scheme for the design variables can be formulated as [59]

$$\alpha_e^{new} = \begin{cases}\max(0,\alpha_e-m) \text{ if } \alpha_e\beta_e^{\eta}\leqslant\max(0,\alpha_e-m) \\ \min(1,\alpha_e+m) \text{ if } \alpha_e\beta_e^{\eta}\geqslant\min(0,\alpha_e+m) \\ \alpha_e\beta_e^{\eta} \text{ otherwise}\end{cases} \tag{28}$$

where m (move) is a positive move-limit that is defined to limit the variable change range, $\eta(=1/2)$ is a numerical damping coefficient, α_e can be variable x or y of the element in this paper, F^{α} can be the objective function of steady-state heat conduction TO problem or eigenvalue optimization problem, and β_e is calculated from the optimality condition, such as:

$$\beta_e = \left(-\frac{\partial F^{\alpha}}{\partial \alpha_e}\right)/\left(\lambda\frac{\partial V}{\partial \alpha_e}\right) \tag{29}$$

where λ is a Lagrangian multiplier that can be found by a bi-sectioning algorithm so that the volume constraint is satisfied. And the sensitivity of the material volume V with respect to α_e is:

$$\frac{\partial V}{\partial \alpha_e} = 1 \tag{30}$$

In the process of multiple materials optimization, it should be noted that the OC method will be employed to update both the variables x and y simultaneously.

5. Numerical examples and discussion

This section presents three numerical examples to show the feasibility and advantage of the proposed multi-objective TO method. Example 1 presents a numerical example to validate the effectiveness of the proposed method. Example 2 changes the objective functions of the proposed method and proves that the proposed multi-objective TO method also works under the situation that considering the mechanical

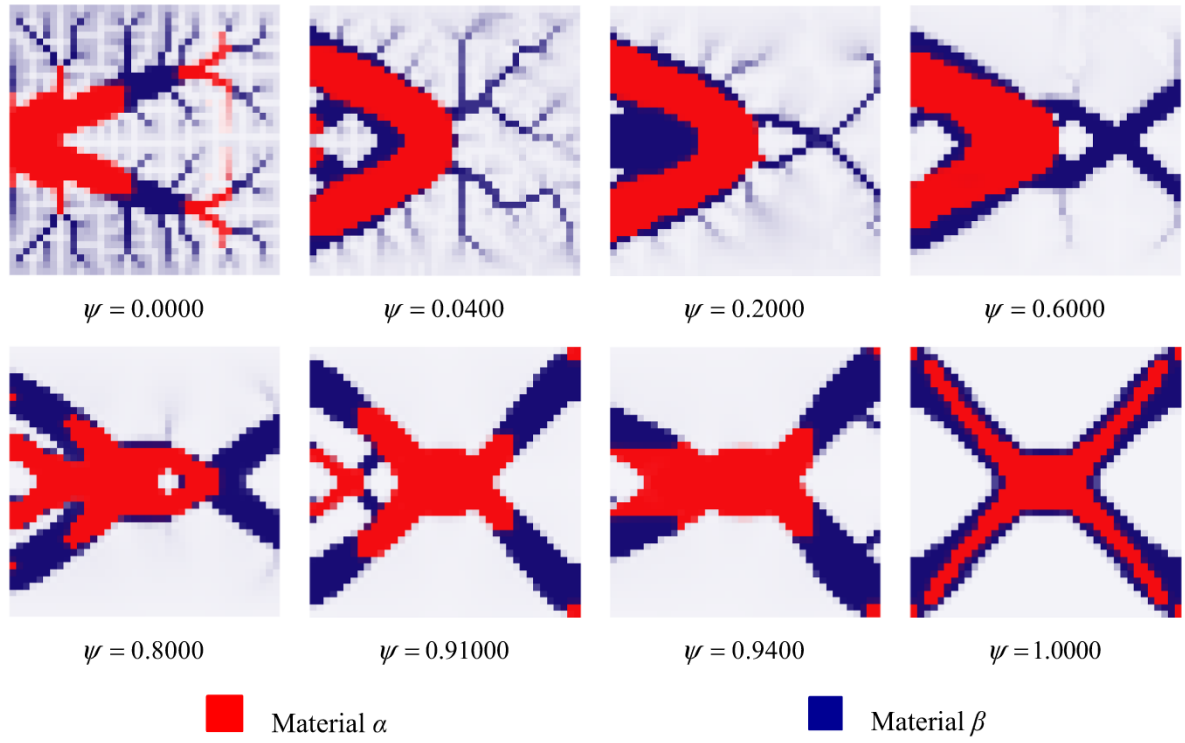

Fig. 2. Optimization result filled by multiple microstructures in Example 1.

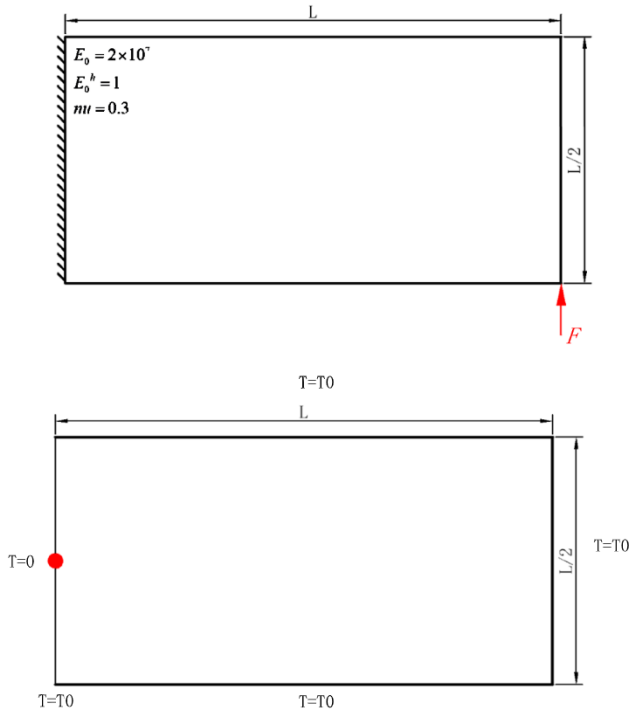

Fig. 3. Load and boundary conditions for the validation case.

compliance and thermal compliance at the same time. Example 3 focuses the optimized results under different material proportions. Furthermore, a self-selected weight sum method that connect the target objective function values with the optimized structures directly is exhibited in Example 3.

5.1. Example 1

Fig. 1 shows the design domain, load and boundary condition of the macrostructure. The properties of the base material have also been shown. The macrostructure is meshed with 40 × 40 linear quadrilateral elements. A distributed heat Q is applied in the entire design domain, which assumes $Q = 0.01\mathrm{W/m^2}$. A small rectangular region is located in the middle of the design domain, where the elements are of much greater mass, mimics the load of the structure [31]. In addition, a rectangular plate with a heat sink is set in the middle of the left side. The final optimal volume should be 50 % of the design domain. The value of the penalization exponent P is equal to 4, and the filter radius is set to be 1.5.

To validate the feasibility of this method, macrostructures in Example 1 will be filled with multiple microstructures, which are material α with area of 50 % and material β with area of 30 % respectively (see Table 1). When the weight coefficient ψ (see Eq. (9)) is set as several fixed values, the results can be seen in Fig. 2.

The results in Fig. 2 demonstrate that the structure evolves smoothly from the full heat conduction to the full natural frequency. When the weight coefficient ψ is set as a value close to 0, the macrostructures are close to the full heat conduction situation with some 'tree-like' branch. As the value of ψ increasing, the macrostructures gradually change toward the full natural frequency situation. It proves the effectiveness of the employment of the multi-objective method.

5.2. Example 2

The multi-objective topology optimization considering the natural frequency and thermal compliance at the same time is presented in this paper. However, the proposed multi-objective in this paper also works when the other objective functions are considering. Following the step of [60], a validation case is presented in this section. In this example, the optimization model considers the mechanical compliance and thermal compliance at the same time. Fig. 3 shows the design domain, load and boundary condition of the macrostructure. The properties of the base

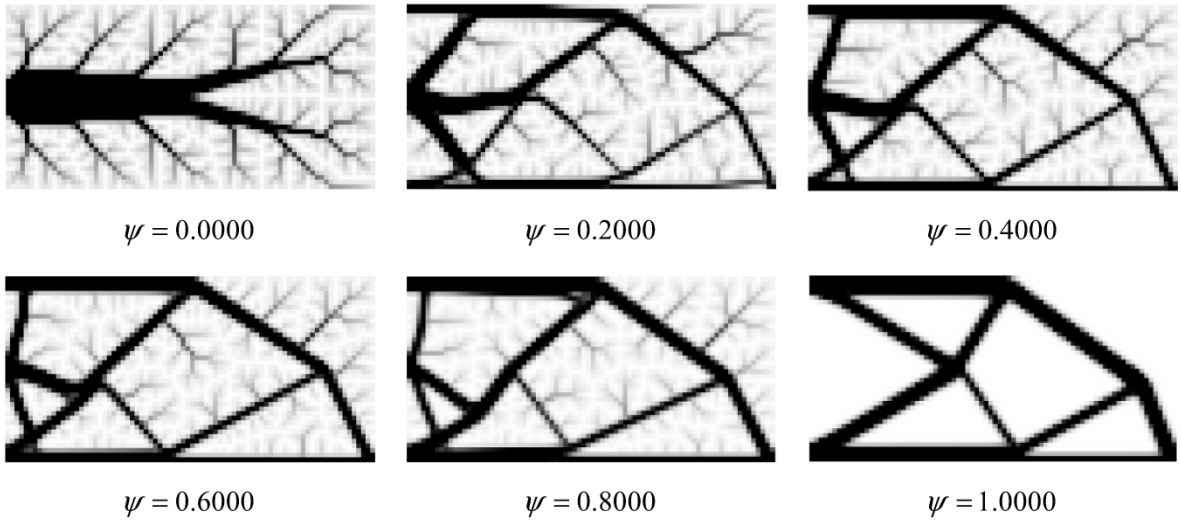

Fig. 4. Optimization result of Loadcase 1 in [60].

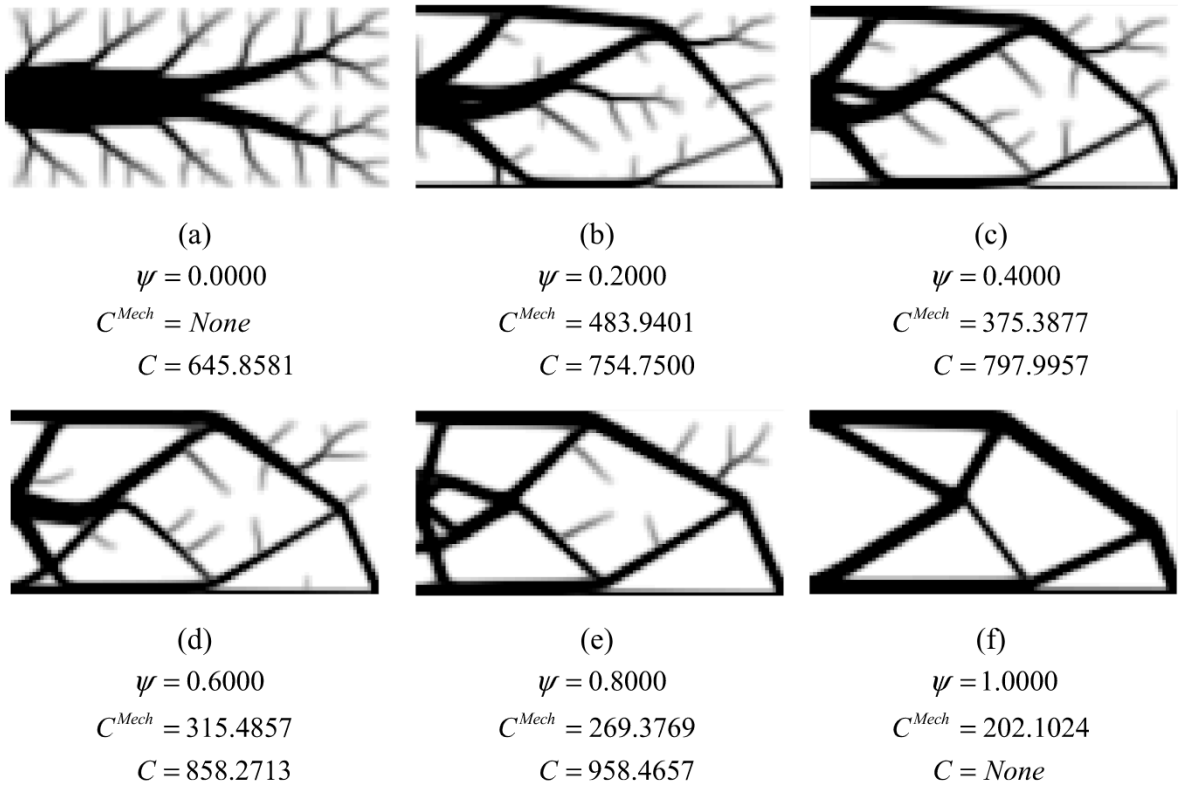

Fig. 5. Optimization result of the validation case (single material situation).

material have also been shown. The macrostructure is meshed with 100×50 linear quadrilateral elements. The final optimized volume should be 30 % of the design domain. A distributed heat Q is applied in the entire design domain, which assumes $Q = 0.001\mathrm{W/m^2}$. A heat sink is set in the middle of the left side. And a force is applied in the bottom right corner of the design domain, which assumes F=2000N. The value of the penalization exponent P is equal to 3, and the filter radius is set to be 1.5.

The weighted-sum method is used to formulate the multi-objective optimization model in this case as:

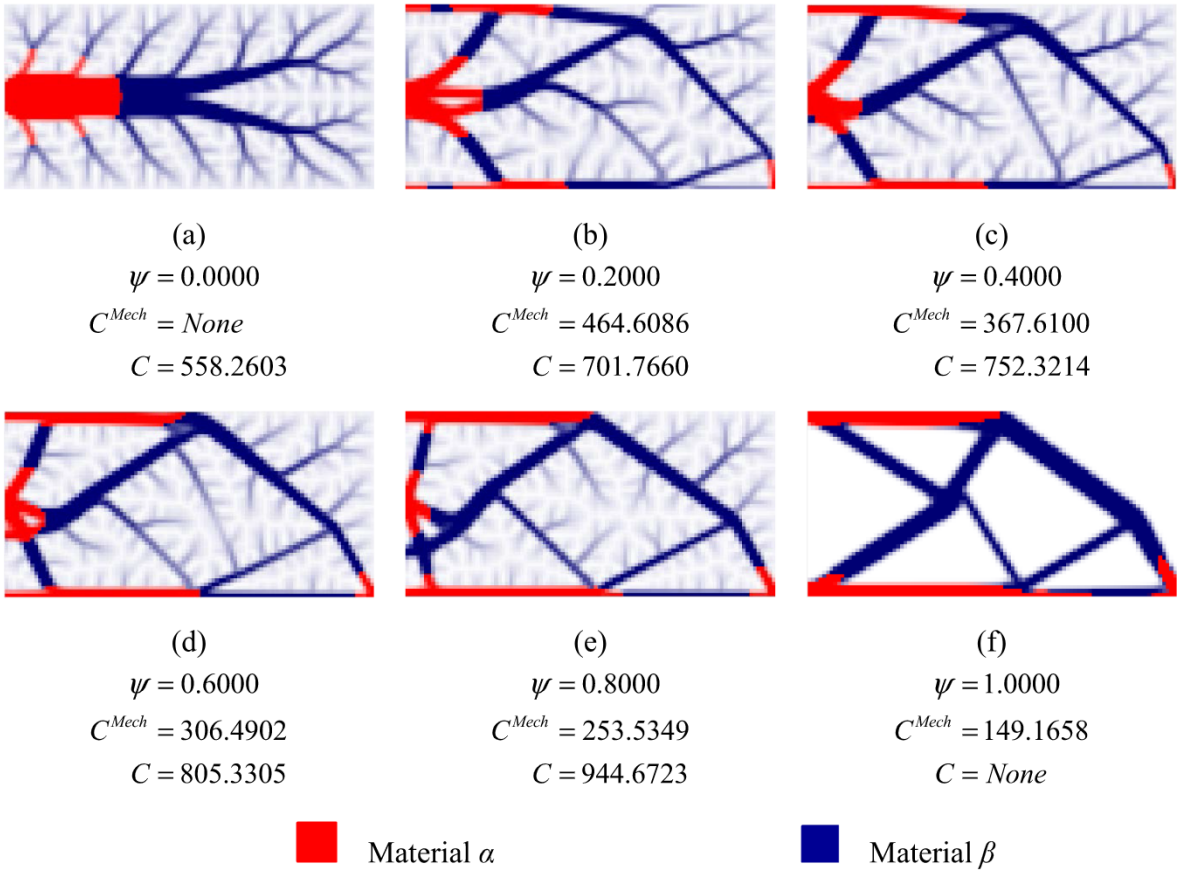

Fig. 6. Optimization result of the validation case (multiple material situation).

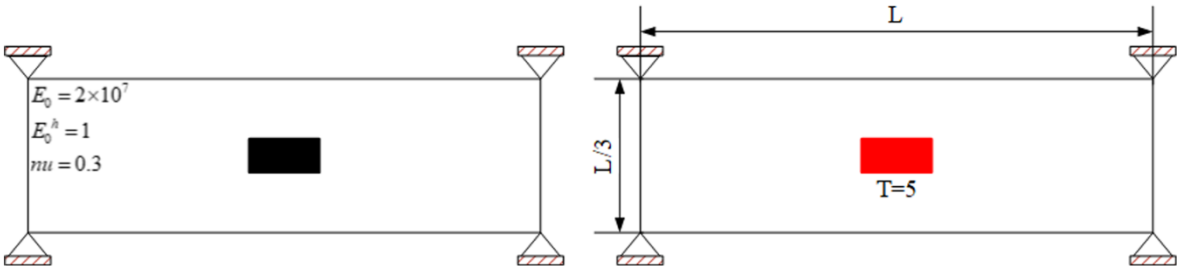

Fig. 7. Load and boundary conditions for Example 3.

$$
\begin{aligned}
\text{Find} \quad & : \quad x = [x_1, x_2, x_3, ..., x_n], \\
& \quad\;\; y = [y_1, y_2, y_3, ..., y_n] \\
\text{Minimize} \quad & : \quad Obj = \psi C^{Mech} + (1-\psi)C \\
\text{Subject to} \quad & : \quad \boldsymbol{K}^h \boldsymbol{T} = \boldsymbol{f}, \\
& \quad\;\; \boldsymbol{K}\boldsymbol{U} = \boldsymbol{F}^{Mech} \\
& \quad\;\; V_{xmax} - \sum_{i=1}^{n} V_i x_i = 0 \\
& \quad\;\; V_{ymax} - \sum_{i=1}^{n} V_i y_i = 0 \\
& \quad\;\; 0 \leqslant x_{min} \leqslant x_i \leqslant x_{max} \leqslant 1 \\
& \quad\;\; 0 \leqslant y_{min} \leqslant y_i \leqslant y_{max} \leqslant 1 \\
& \quad\;\; 0 \leqslant \psi \leqslant 1
\end{aligned}
\tag{31}
$$

where $\boldsymbol{U}$ is global displacement, $\boldsymbol{F}^{Mech}$ is the force vector, C^{Mech} is the mechanical compliance, which can be calculated as:

$$
C^{Mech} = \boldsymbol{U}^T \boldsymbol{K}\, \boldsymbol{U} = \sum_{i=1}^{N} \boldsymbol{u}_e^T \boldsymbol{k}_e \boldsymbol{u}_e \tag{32}
$$

where $\boldsymbol{u}_e$ and $\boldsymbol{k}_e$ are the element displacement vector and stiffness matrix, respectively.

The sensitivity is needed to update the variables by applying the OC method. The sensitivity of heat conductive TO can be seen in Eq. (18) and Eq. (19). According to the chain rule and the adjoint method, the derivative of the mechanical compliance with respect to variables x_{ij} and y_{ij} can be written as

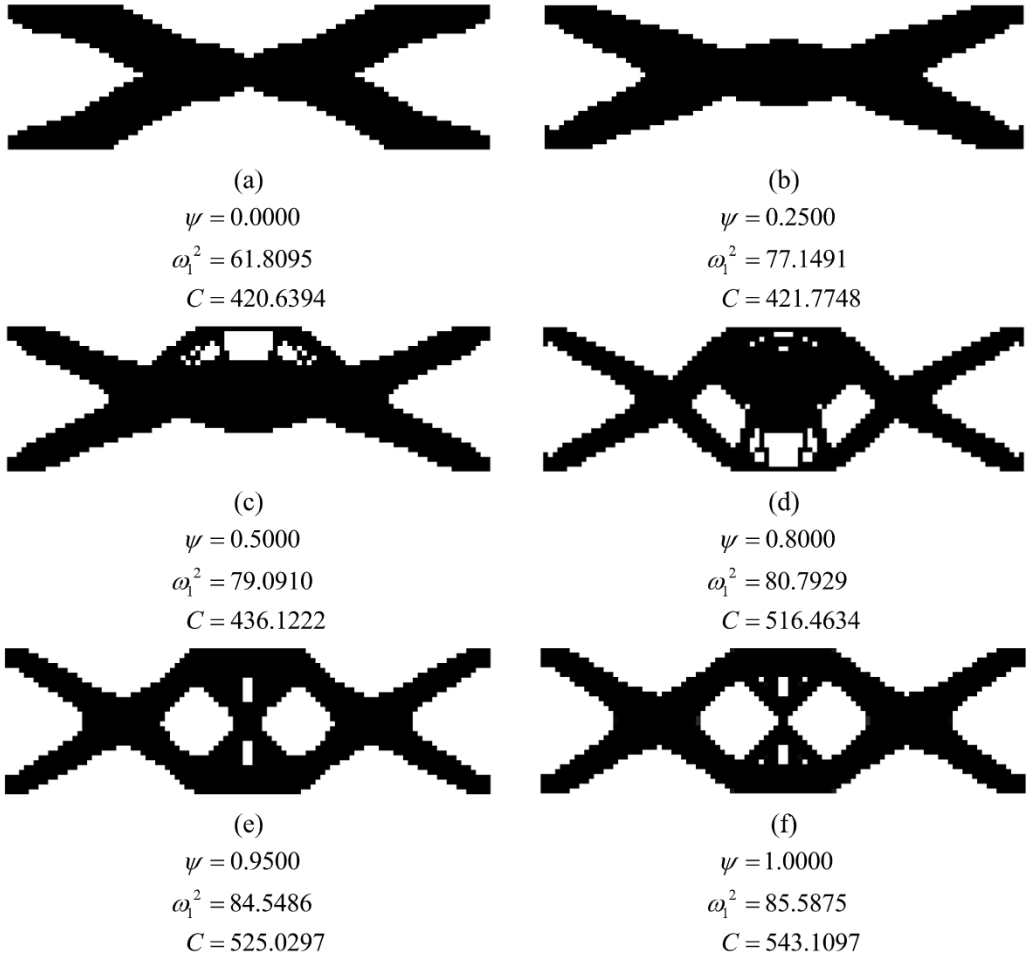

Fig. 8. Optimization result of case 1.

$$\begin{aligned}\frac{\partial C^{Mech}}{\partial x_i} &= -\boldsymbol{u}_e^T \frac{\partial \boldsymbol{K}_e}{\partial x_i}\boldsymbol{u}_e \\ &= -\boldsymbol{u}_e^T \int_v \boldsymbol{B}\,\frac{\partial \boldsymbol{D}_e}{\partial x_i}\boldsymbol{B}\,dv\boldsymbol{u}_e \\ &= -\boldsymbol{T}_e^T \int_v \boldsymbol{B}\,Px_i^{P-1}\left\{y_i^P D_0^2 + \left[1-(y_i)^P\right]D_0^1\right\}\boldsymbol{B}^h dv\boldsymbol{T}_e \\ &= -\boldsymbol{T}_e^T x^{-1} \int_v \boldsymbol{B}\,Px_i^P\left\{y_i^P D_0^2 + \left[1-(y_i)^P\right]D_0^1\right\}\boldsymbol{B}^h dv\boldsymbol{T}_e \\ &= -\boldsymbol{T}_e^T x^{-1} \int_v \boldsymbol{B}\,PD_e\boldsymbol{B}^h dv\boldsymbol{T}_e \\ &= -Px_i^{-1}\boldsymbol{u}_e^T\boldsymbol{K}_e\boldsymbol{u}_e\end{aligned} \tag{33}$$

$$\begin{aligned}\frac{\partial C^{Mech}}{\partial y_i} &= -\boldsymbol{u}_e^T \frac{\partial \boldsymbol{K}_e}{\partial y_i}\boldsymbol{u}_e \\ &= -\boldsymbol{u}_e^T \cdot \int_v \boldsymbol{B}\,\frac{\partial \boldsymbol{D}_e}{\partial y_i}\boldsymbol{B}\,dv\cdot\boldsymbol{u}_e \\ &= -P\cdot x_i^P \cdot y_i^{P-1}\cdot\boldsymbol{u}_e^T\cdot\left(\boldsymbol{K}_2 - \boldsymbol{K}_1\right)\cdot\boldsymbol{u}_e\end{aligned} \tag{34}$$

Combining with Eq. (18) and Eq. (19), the sensitivity of the multi-objective function can be directly derived as:

$$\frac{\partial Obj}{\partial x_i} = \psi\frac{\partial C^{Mech}}{\partial x_i} + (1-\psi)\frac{\partial C}{\partial x_i} \tag{35}$$

$$\frac{\partial Obj}{\partial y_i} = \psi\frac{\partial C^{Mech}}{\partial y_i} + (1-\psi)\frac{\partial C}{\partial y_i} \tag{36}$$

The optimized structures in [60], which are shown in Fig. 4, are used as the standard to prove the feasibility of the proposed method.

In this case, the structures are filled with material β with area of 30 % and the optimized structures can be seen in Fig. 5.

The optimized results above show that the topology of the optimized structures change significantly with the change of the weight coefficient. Besides, the optimized structures in Fig. 5 has similar structural characteristics to that in Fig. 4. When the weight coefficient is equal to 0 or 1, the proposed multi-objective optimization method degenerates into a single-objective optimization method. Therefore, in the cases of $\psi =$ 0.0000 and$\psi = 1.0000$, only the value of the objective function with a weight coefficient of 1 is calculated, and the value of the objective function with a weight coefficient of 0 is represented by *None*.

To show the difference in macroscopic structural properties when filled by multiple microstructures, numerical example with the same loads and boundary conditions is performed. Material β with area of 30 % and material α with area of 50 % are used for filling, and the volume ratio of material β to material α is 2:1 ($v_{\beta:\alpha}$=2). The optimized results can be seen in Fig. 6.

Comparing with Fig. 5, the structures in Fig. 6 has better performance in both the mechanical compliance and thermal compliance. Therefore, we can draw a conclusion that the proposed multi-objective topology optimization method is still feasible under the situation that considering both mechanical compliance and thermal compliance at the same time. Meanwhile, the optimized structures with better performance can be obtained by applying the MMTO.

Here in example 2, a typical numerical example of multi-objective topology optimization is selected to verify the proposed method. Besides, we expanded this numerical example to multiple materials situation to better demonstrate the advantages of the optimized structures

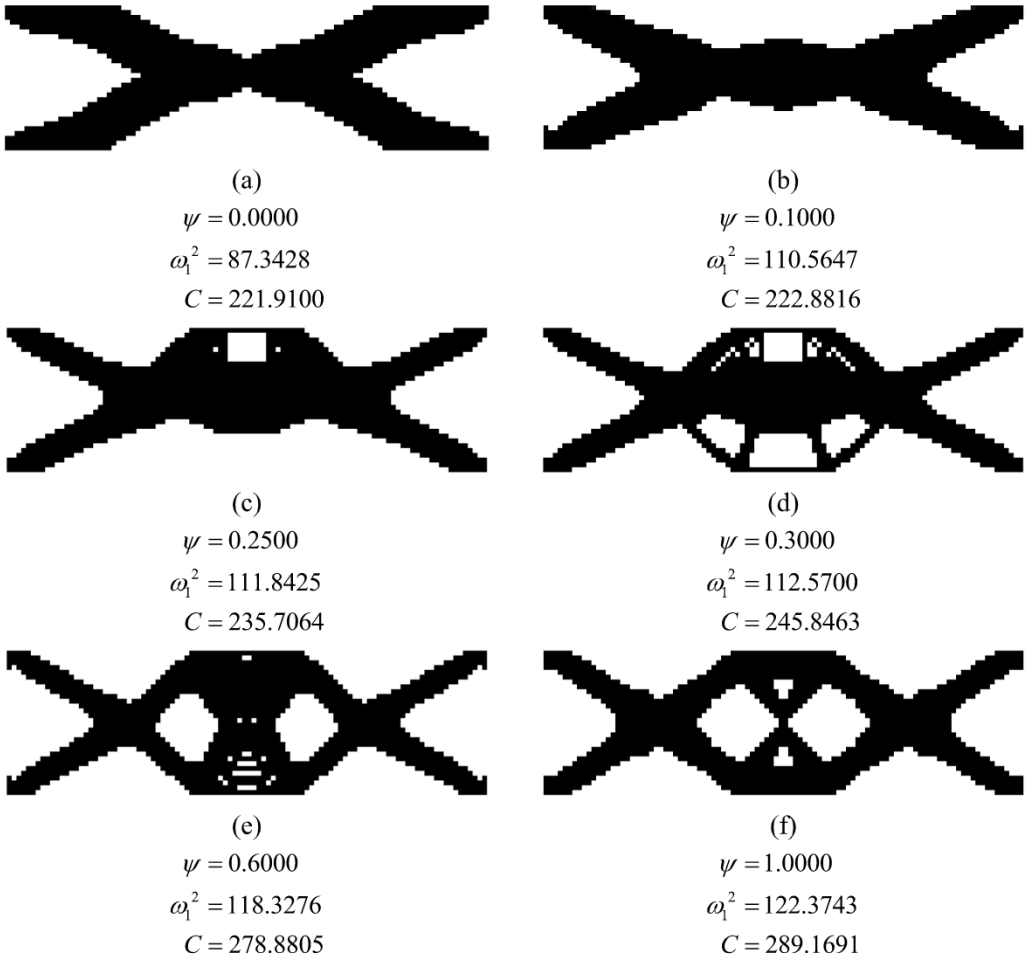

Fig. 9. Optimization result of case 2.

filling with multiple materials. Similar works can be found in [61], in which the constraints and loading conditions of the design domain are different from the examples above.

5.3. Example 3

Fig. 7 shows the loads and boundary conditions of the design domain. The properties of the base material have also been shown. The macrostructures are meshed with 100×30 linear quadrilateral elements. A small rectangular region is located in the middle of the design domain, where the elements are of much greater mass to mimics the structural load [31], while a rectangular plate with a heat source is set in the same place. Similar to Example 1, the optimal volume should be 50 % of the design domain. The value of the penalization exponent P is equal to 4, and the filter radius is set to be 0.75.

5.3.1. Filled by single-phase material

To show the advantage of the MMTO method, firstly, assuming that the macrostructures are filled by single-phase microstructure, which contains three cases. In case 1, the structure is filled by material β with area of 30 %. In case 2, the structure will be filled by material β with area of 50 % to show the influence of area to the values of objective functions. In case 3, the structure is filled by material α with area of 50 % to show the influence of the lay-out of lattice to the values of objective functions. In all the cases, several weight coefficients are selected and multi-objective topology optimization was carried out. The result can be seen in Figs. 8 and 9.

As area change from 30 % to 50 %, the lattice will have better performances in both the heat conduction and the natural frequency. Comparing with the results in Fig. 8, macrostructures in Fig. 9 have higher natural frequency and lower thermal compliance.

In Fig. 10, the lay-out of macrostructures and the process of structural changing is similar to that of Fig. 9. From the perspective of objective functions, material α performs better in heat conduction while material β behaves better in natural frequency. For example, when the weight coefficient ψ is equal to 0.6, the structure in Fig. 9 has higher natural frequency and thermal compliance comparing to the structure in Fig. 10. This kind of difference becomes bigger as the value of weight coefficient ψ changes from 0 to 1.

5.3.2. Filled by multiple materials

To show the difference of macroscopic structural properties when filled by multiple lattice materials, numerical example with the same loads and boundary conditions is performed. To demonstrate the relationship between the optimized results and material proportion, it contains two cases: (1) the volume ratio of material β to material α is equal to 4:1, i.e. $v_{\beta:\alpha}$=4 (case 4), and (2) the volume ratio of material β to material α is 2:3, $v_{\beta:\alpha}$=2/3 (case 5). In this section, area of material β is equal to 30 % and area of material α is equal to 50 %. In case 4 and case 5, to analysis the convergence performance of the proposed method, parameter *change* is used as the basis of iterative convergence. The iteration converge when *change* is less than 10^{-5}, which can be calculated by using the following formula:

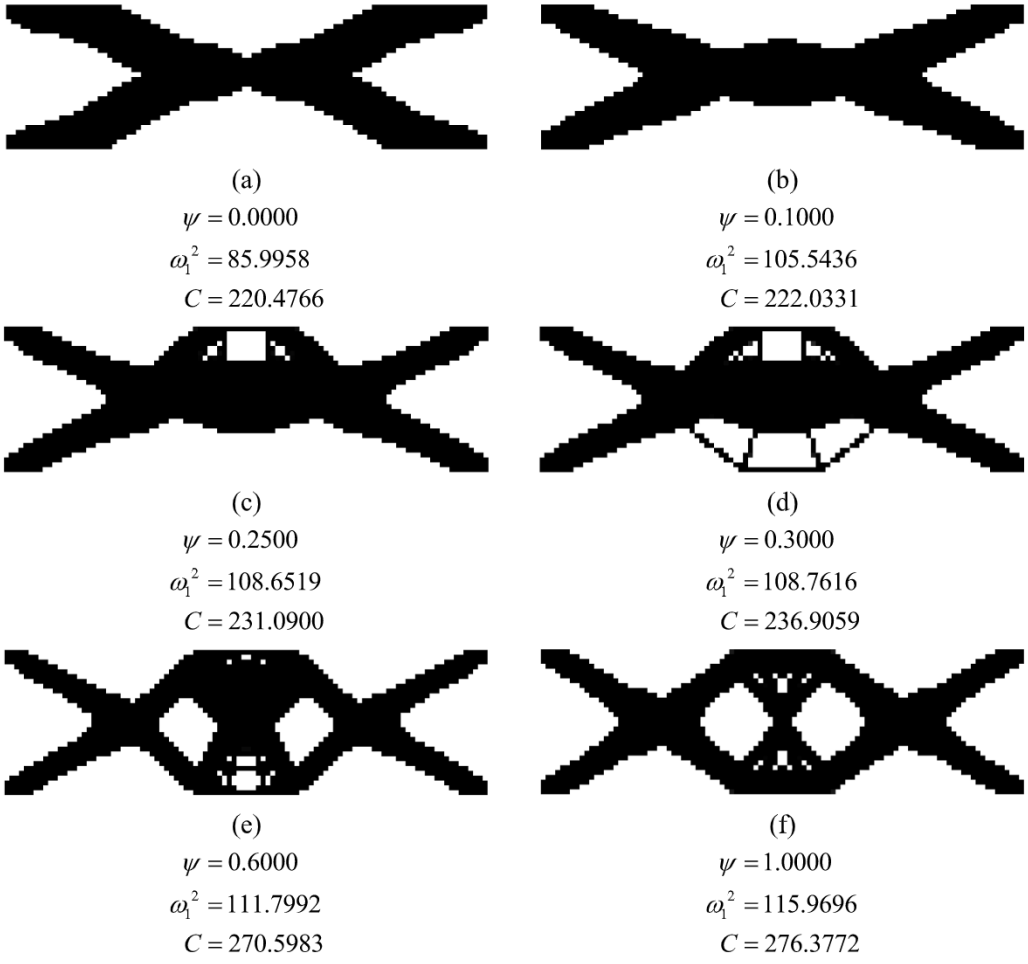

Fig. 10. optimization result of case 3.

$$change = \frac{\left|\sum_{loop-9}^{loop-5} F_i - \sum_{loop-4}^{loop} F_j\right|}{\left|\sum_{loop-4}^{loop} F_j\right|} \tag{37}$$

where *loop* and *loop-i* represent number of iteration.

For case 4 with $v_{\beta:\alpha}$=4, the optimized results of some fixed coefficient ψ can be obtained as Fig. 11.

From the perspective of the objective function values, it is closer to the situation of Fig. 8 because of the dominant quantity of material β. Similarly, for case 5 with $v_{\beta:\alpha}$=2/3, the results can be seen in Fig. 12.

Before the analysis of the optimized result, a necessary validation of the mesh sensitivity and the performance of convergence is presented here. The following analysis of the proposed method are made with the volume ratio of $v_{\beta:\alpha}$=2/3.

Firstly, to validate the performance of the method against mesh sensitivity, two other mesh are applied here, which are 150×45 and 200×60 respectively. The optimized result can be seen in Fig. 13.

As can be seen, optimized structures in Fig. 13 are similar to that in Fig. 12. This proves that the proposed method has a good performance against mesh sensitivity.

Secondly, as shown in Fig. 11 and Fig. 12, for most of the weight coefficients, convergence occurs at between 25 and 50 iterations. When the weight coefficients are around 0.5, it may need more iterations to reach convergence. This proves that the proposed method has good performance in convergence.

As for the optimized results, the optimized structures in Fig. 12 are closer to those of Fig. 10. Combining with Fig. 11, we can draw a conclusion that the optimized result depends mostly on the properties of the abundant material. By changing the proportion of different materials, the MMTO can enlarge the result domain.

To prove this, ranging the weight coefficient ψ from 0 and 1, over 400 sample points are taken to establish the result domain of the all cases above. The scatter diagram is used to describe the result domain, which can be seen in Fig. 14:

As shown in Fig. 14, firstly, by employing the multiple materials method, the result domain with a smoother change are obtained. While in the case filling by single-phase material, the value of thermal compliance might vary dramatically in a small interval. It means that the employment of multiple materials TO provides the macrostructures with a more continuous optimized results.

Secondly, the use of multiple materials TO expands the result domains. As seen from the Fig. 14, area A and area D represent the allowable design domains filled by material β and material α, respectively. Points above the boundary can be obtained by changing the value of ψ, while points in the design domains can be obtained by decreasing the final optimized volume of the structure or by using a base material with slightly inferior properties to fill the lattice. Area B and area C represent the allowable design domains of case 4 and case 5 respectively, which cover extra design domains outside the area A and area D. By changing the proportion of materials, the result domains of multiple materials optimization will move to that of single-material optimization with dominant quantity. When ranging the proportion of materials $v_{\beta:\alpha}$ from ∞ to 0 (from single-phase material β to single-phase material α), area E in Fig. 15 can be obtained, which is an overall additional design domain when using the MMTO method comparing with area A and area D.

The optimization results can be preserved by the fitting function of

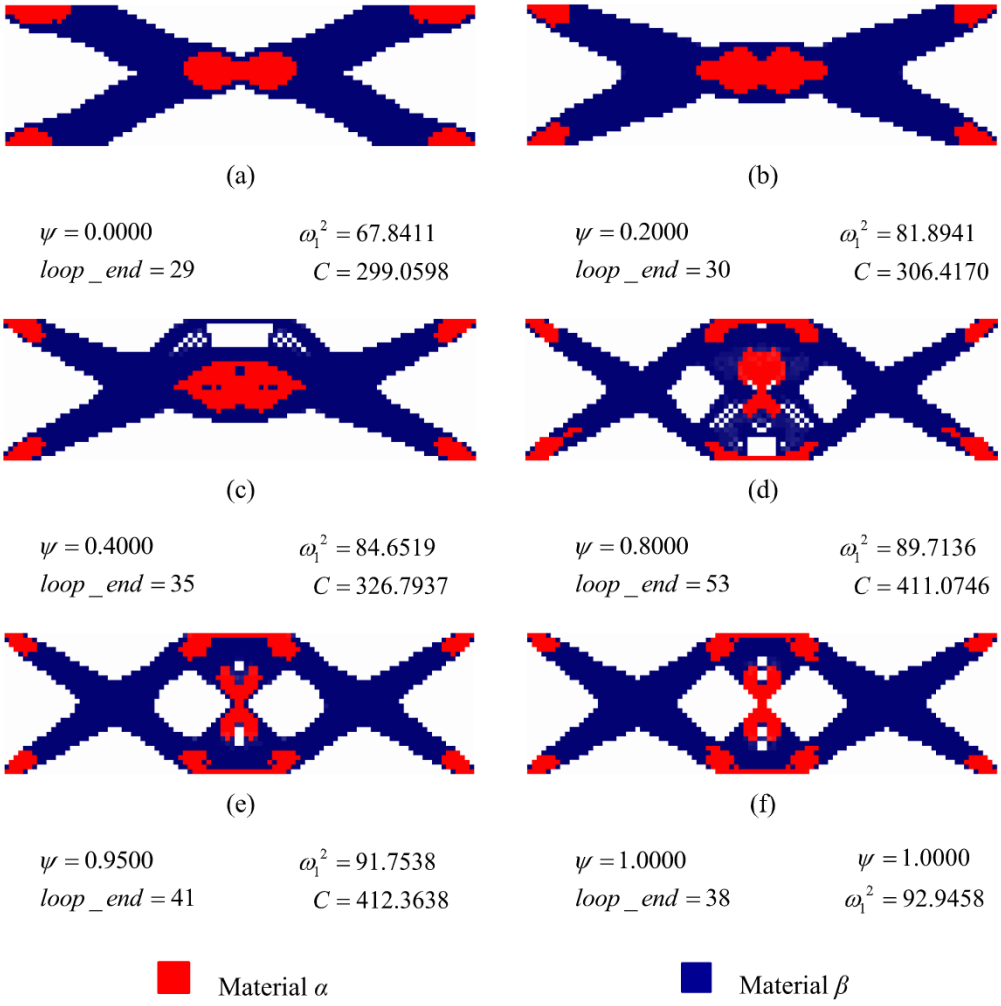

Fig. 11. Optimization result of case 4 with $v_{\beta:\alpha} = 4$.

the result domain. Taking case 5 as an example, the result domain can be seen in Fig. 16.

The relationship between the natural frequency and the heat potential capacity can be described using the fitting function, which can be written as:

$$C = 0.002631\cdot(\omega_1^2)^3 - 0.5364\cdot(\omega_1^2)^2 + 35.02\cdot(\omega_1^2) - 465.4 \tag{38}$$

where the R-square is equal to 0.988. It means that in most of the situation, every point selected on the curve has an actual structure that corresponds to it. Similarly, the relationship between the weight coefficient and the two objective functions can be established in the same way, which can be seen in Fig. 17 and the fitting functions can be written as:

$$C = -166.8\psi^3 + 315.4\psi^2 - 71.81\psi + 254.7 \tag{39}$$

$$\omega_1^2 = 37.47\psi^3 - 75\psi^2 + 64.49\psi + 77.38 \tag{40}$$

which the R-square is equal to 0.9919 and 0.9776, respectively.

5.3.3. A self-selected weight sum method

A self-selected weight sum method that provides a new way to obtain optimized structures with given objective values is presented here. This method is based on the fitting functions of the result domains and the bisection method. The procedure of employing the method can be depicted in Fig. 18, and the algorithm implementation is explained in Table 3.

The objective functions will vary by changing the value of the material proportion. In the procedure of employing the self-selected weight sum method, the material proportion interval will be subdivided in each iteration and changing the material proportion according to the objective functions value of the target result point.

Herein, an example is presented here to further express the procedure of employing the method above. Material α with area of 50 % and material β with area of 30% are used for filling. Assuming that the target objective function value are ${\omega_1}^2 = 75, C = 350$. The acceptable error *err* of the result point to the target result point is set as 5%. As seen from the Fig. 14, the result domain of material α and material β can be obtained. It can be shown in Fig. 19.

The initial design domain is separated into several subdomains by the result domains of multiple material situations. As seen from Fig. 19 the target result point can be found between the result domain of single-phase material β and the result domain of multiple materials situation that $v_{\beta:\alpha}$=4. To get the target result point, the volume of material β needs to be increased compared with the case of $v_{\beta:\alpha}$=4.

Using the bisection method, increasing the volume of material β, the result domain can be seen in Fig. 20, when $v_{\beta:\alpha}$ is set as 9 temporarily, the result domain is not close enough to the target result point. The fitting function under this situation can be written as:

$$C = -0.002821\cdot(\omega_1^2)^3 + 1.048\cdot(\omega_1^2)^2 - 107.3\cdot(\omega_1^2) + 3658 \tag{41}$$

When ${\omega_1}^2 = 75$, according to Eq. (41), $C = 315.3906$. The error in this situation is equal to 9.888%, which is larger than the acceptable value.

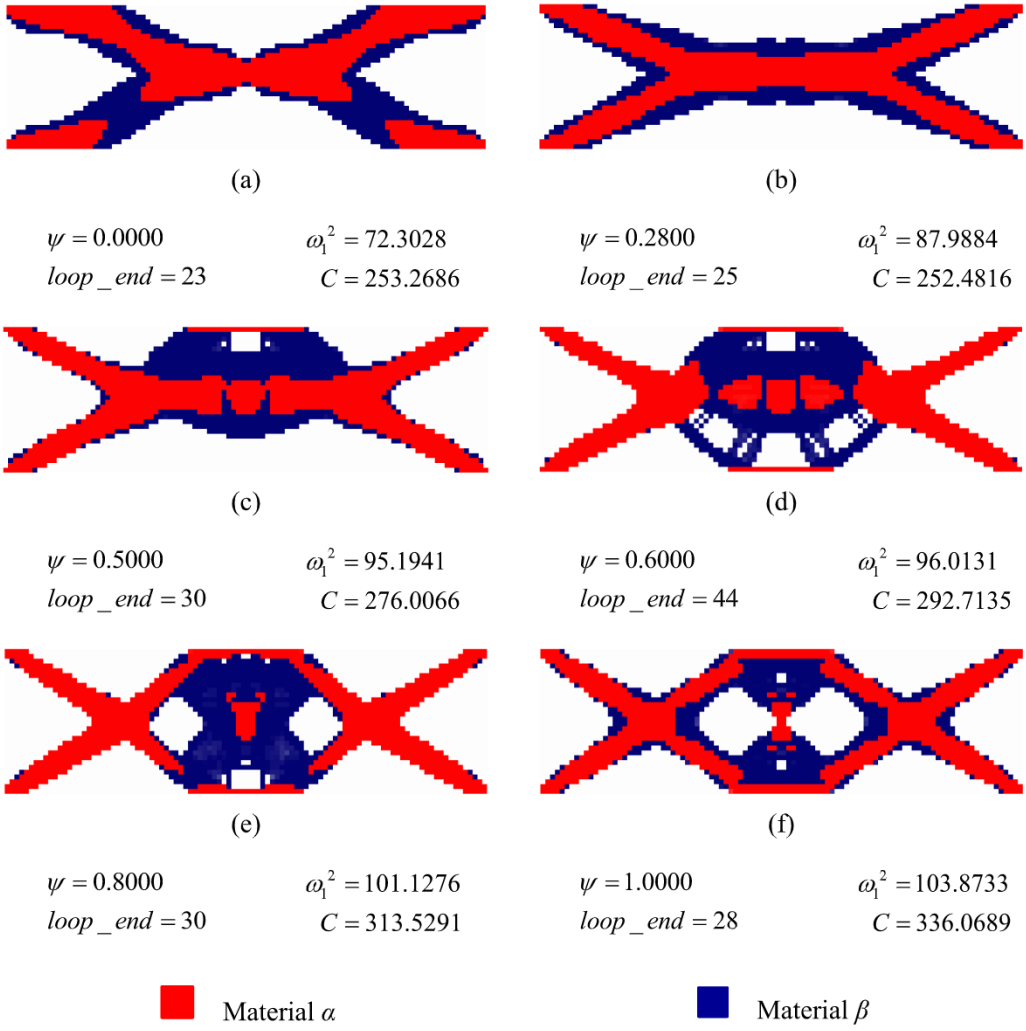

Fig. 12. Optimization result of case 5 with $v_{\beta:\alpha} = 2/3$.

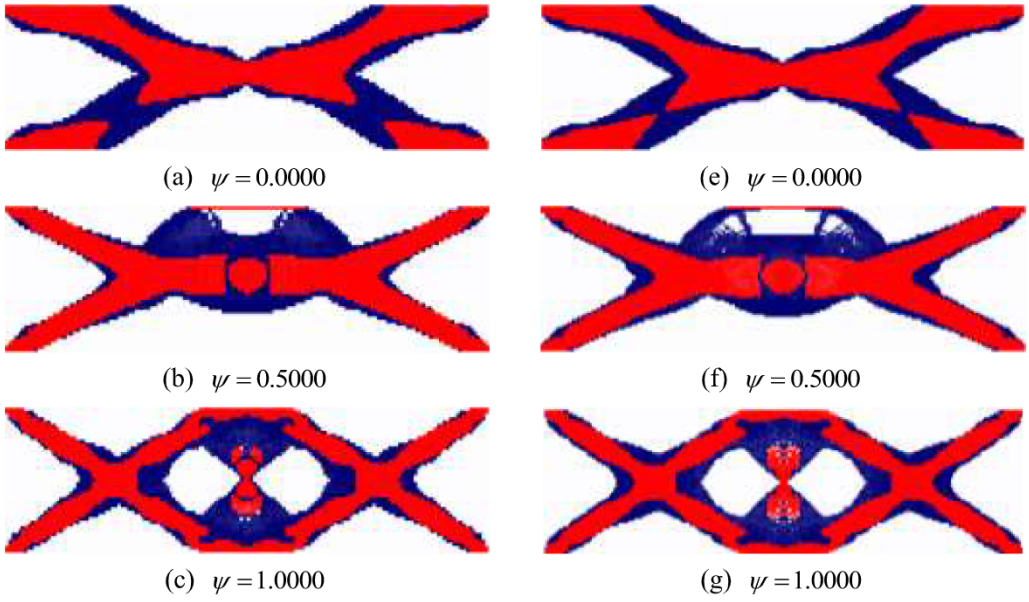

Fig. 13. Optimization result of the validate case 1 with $v_{\beta:\alpha}$=2/3 (Fig. 9(a) to Fig. (c) are the optimized structures under the mesh scale of150 × 45, while the other figures are the optimized structures under the mesh scale of 200 × 60).

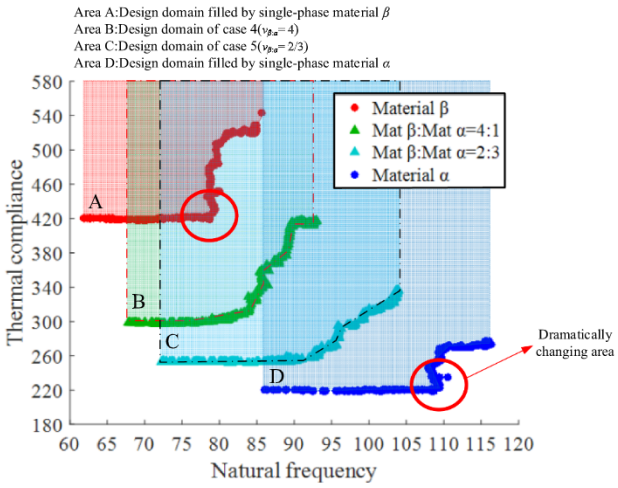

Fig. 14. Optimization result domain of several cases.

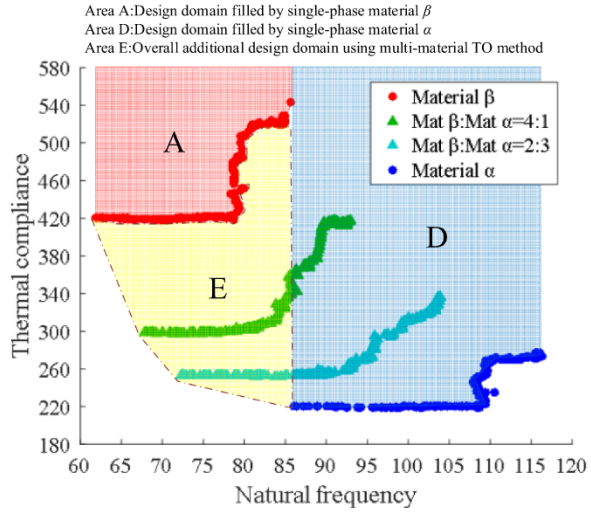

Fig. 15. Optimization result domain and the overall extra design domain.

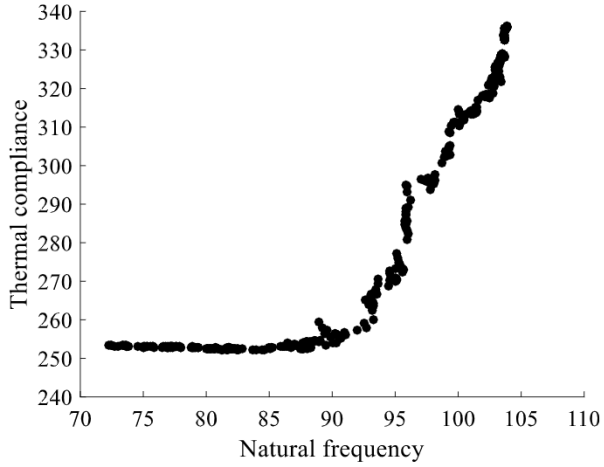

Fig. 16. Optimization result domain of case 5.

Keep increasing the volume of material β, whose material proportion is set as 19, the result can also be seen in Fig. 20. Each result point has its corresponding objective function value, weight coefficient of each objective function and material proportion. The relationship between objective functions and the relationship between objective functions and weight coefficients can be expressed by fitting functions. Eq. (42) shows the relation between thermal compliance and the natural frequency, while Eq. (43) and Eq. (44) represent the relation between the objective and weight coefficients. The fitting function under this situation can be written as:

$$C = 0.0006281\cdot(\omega_1^2)^3 + 0.2583\cdot(\omega_1^2)^2 - 46\cdot(\omega_1^2) + 2072 \tag{42}$$

$$C = -383.1\psi^3 + 626.8\psi^2 - 131.5\psi + 342.2 \tag{43}$$

$$\omega_1^2 = 44.82\psi^3 - 84.06\psi^2 + 60.4\psi + 68.06 \tag{44}$$

When ${\omega_1}^2 = 75$, according to Eq. (42), $C = 339.9172$, which is close to the target result point. Referring to the Eq. (43) or Eq. (44), the weight coefficient can be obtained, which is equal to 0.2243. Put the value of ψ into the main algorithm, the objective functions are ${\omega_1}^2 = 77.3812, C = 341.2140$ respectively. This error of ${\omega_1}^2$ and C between this situation and the target result point is equal to 3% and 2.5% respectively, which is acceptable. And the optimized structure can be in Fig. 21.

As seen from the above example, the weight coefficient and the optimized structure can be obtained directly by employing the self-selected weight sum method. When the acceptable error is set as 5%, in most cases, the target result point can be obtained after 3 iterations. It can be smaller when the target result point is placed in a material proportion interval that the result domains are closer to each other.

In example 1 to 3, two kinds of microstructures with isotropic material properties are used for filling. However, the proposed multi-objective optimization method also works for orthotropic or anisotropic materials, where only the constitutive equations of materials are different from that of isotropic materials.

6. Conclusions

This paper has proposed a multi-objective optimization algorithm to design a structures with lower thermal compliance and higher natural frequency at the same time. It is based on the steady-state heat conduction TO and eigenvalue TO. The homogenization method is used to calculate the effective properties of the microstructures used for filling in the macrostructures. To prove the feasibility of this algorithm, several numerical examples is presented in this paper. The following conclusions can be drawn by analyzing the result of numerical examples:

(1) The multi-objective optimization method is feasible in both the single-phase material and multi-phase material situations. It succeeds in providing the macrostructure with a lower thermal compliance and higher natural frequency. Besides, the proposed method is also suitable for the situation that considering the mechanical compliance and thermal compliance at the same time. A more continuous optimized results can be obtained by employing the multiple materials topology optimization;
(2) The result domains are largely expanded by using the MMTO method. The result points between the single-material result domain can be obtained by changing the proportion of the materials;
(3) Besides, a self-selected weight sum method that is based on the result domains of both single-phase and multiple materials situations is proposed. An example is presented to show the procedure of employing the method. The result demonstrates that the target result point can be found using this method within a certain error range. This method provides a more flexible way to get the optimized structures directly after the requirement is determined.

Due to the limitation of time, in this paper, only the concept of the

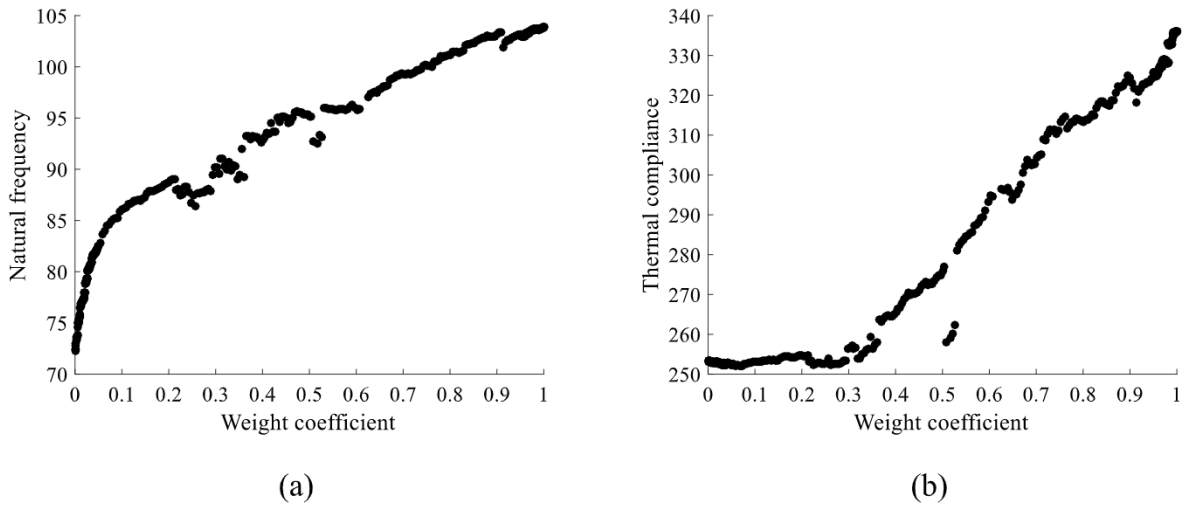

Fig. 17. Relationship between two objectives function.

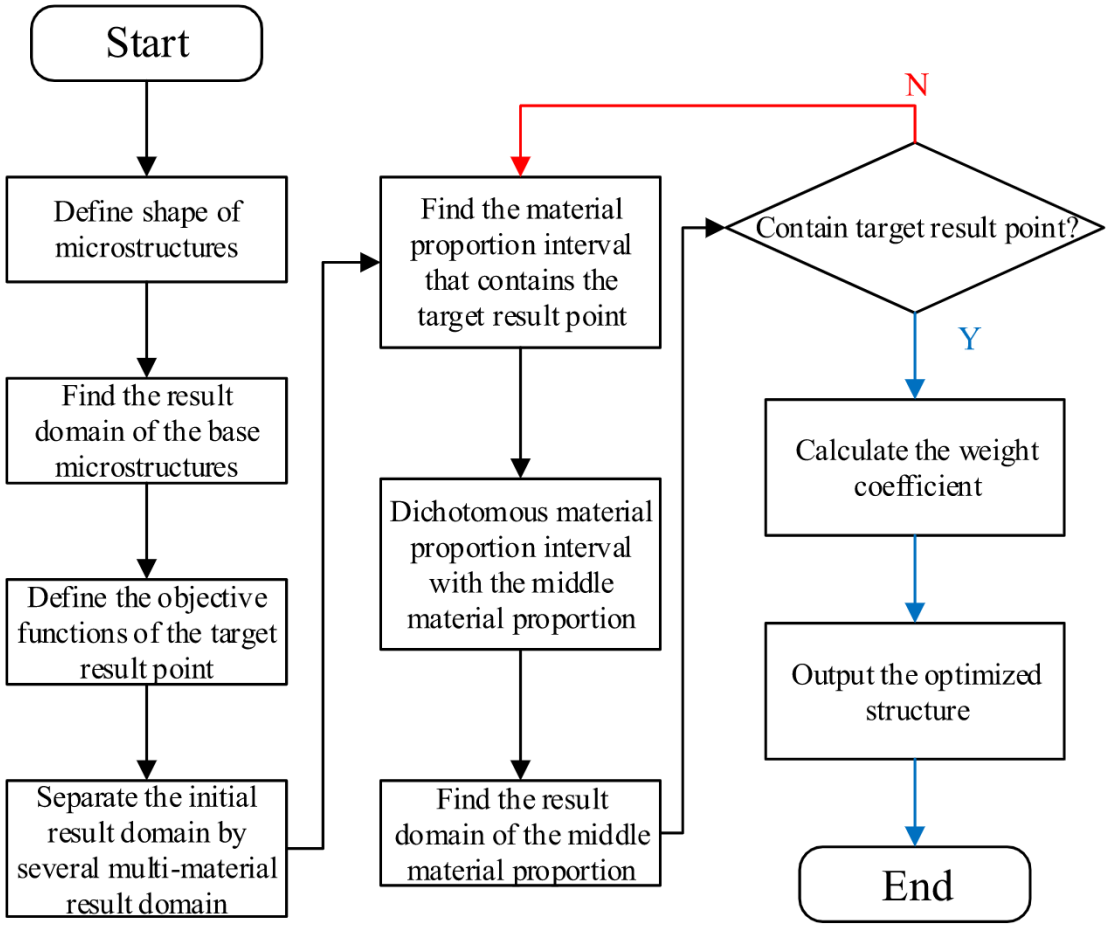

Fig. 18. Flow chart of the self-selected weight sum method.

method and some simple numerical examples in 2D domains are presented. In future, the following works are needed to be done with the purpose of improving the method. Firstly, some extended applications in plate, shell and solid problems will be done in future studies. Besides, the multi-objective optimization algorithm is expected to combine with acceleration algorithms [62,63] and artificial intelligence algorithms [64] to improve the computational efficiency and provide a more precise method of selecting weight coefficient.

CRediT authorship contribution statement

Wenjun Chen: Methodology, Investigation, Data curation, Writing – original draft. **Yongfeng Zheng:** Conceptualization, Supervision, Writing – review & editing. **Yingjun Wang:** Supervision, Writing – review & editing.

Table 3
The self-selected weight sum method.

	The self-selected weight sum method
1	Define the basic parameters of TO, and select the filling materials
2	Given the target values of each objective, and define the expected error *err*
3	Initialize the biggest value of the difference between each objective function and the target value *b-err* to *err* + 0.1
4	Calculate elastic matrixes and thermal elastic matrixes of the filling materials
5	Find out the result domain of each filling material and form up the overall feasible result domain
6	if *b-err* > *err* then
7	Adjust the material proportion and find out the result domain.
8	Solve the approximate result point inversely
9	Calculate *b-err*
10	else
11	Solve the weight coefficient of each objective inversely, and obtained the optimized structure.
12	end if
13	Return the optimized result

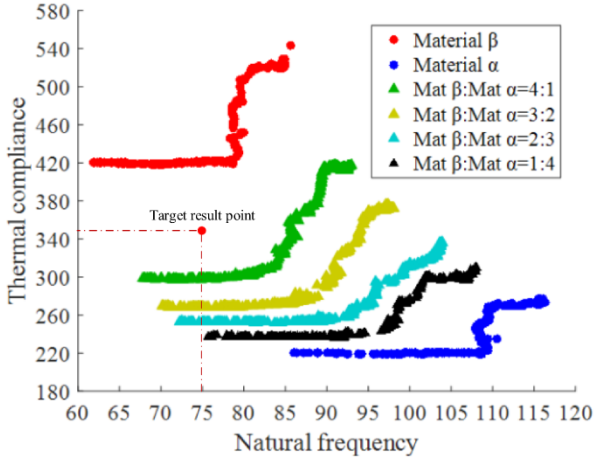

Fig. 19. Result domains and the target result point.

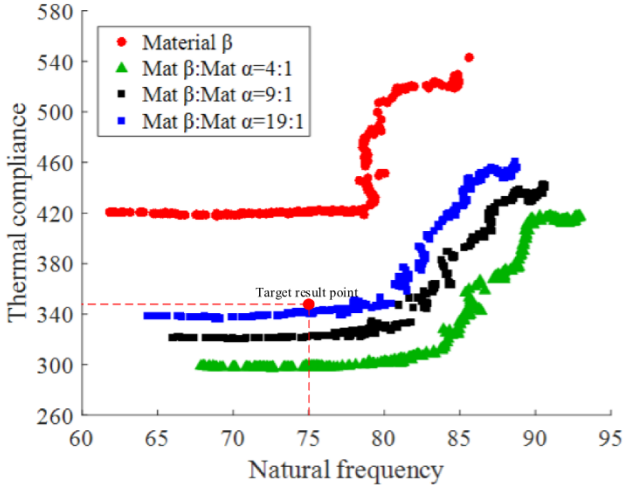

Fig. 20. The target material proportion interval.

Declaration of Competing Interest

The authors declare that they have no known competing financial interests or personal relationships that could have appeared to influence the work reported in this paper.

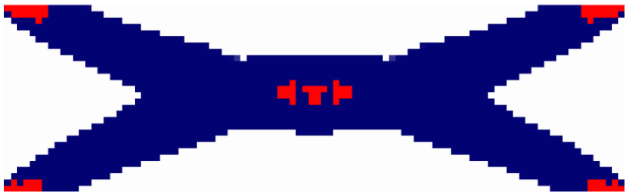

Fig. 21. The optimized structure of the target result point.

Data availability

Data will be made available on request.

Acknowledgment

This work has been supported by National Natural Science Foundation of China [No. 52075184], Guangdong Basic and Applied Basic Research Foundation [No. 2019A1515011783], National Key R&D Program of China [No. 2020YFB1708300], Open-funding Project of State Key Laboratory of Digital Manufacturing Equipment and Technology (Huazhong University of Science and Technology) [No. DMETKF2021020]. These supports are gratefully acknowledged.

References

[1] Bendsøe MP, Kikuchi N. Generating optimal topologies in structural design using a homogenization method. Comput Method Appl M 1988;71(2):197–224.
[2] Sigmund O. A 99 line topology optimization code written in Matlab. Struct Multidiscip O 2001;21(2):120–7.
[3] Xie YM, Steven GP. A simple evolutionary procedure for structural optimization. Comput Struct 1993;49(5):885–96.
[4] Allaire G, Jouve F, Toader A-M. Structural optimization using sensitivity analysis and a level-set method. J Comput Phys 2004;194(1):363–93.
[5] Deng X, Wang Y, Yan J, Liu T, Wang S. Topology optimization of total femur structure: application of parameterized level set method under geometric constraints. J Mech Design 2016;138(1):011402.
[6] Guo X, Zhang W, Zhong W. Doing topology optimization explicitly and geometrically—a new moving morphable components based framework. J Appl Mech 2014;81(8).
[7] Zhang W, Song J, Zhou J, Du Z, Zhu Y, Sun Z, et al. Topology optimization with multiple materials via moving morphable component (MMC) method. Int J Numer Meth Eng 2018;113(11):1653–75.
[8] Zuo W, Saitou K. Multi-material topology optimization using ordered SIMP interpolation. Struct Multidiscip O 2017;55(2):477–91.
[9] Lindgaard E, Dahl J. On compliance and buckling objective functions in topology optimization of snap-through problems. Struct Multidiscip O 2013;47(3):409–21.
[10] Nørgaard S, Sigmund O, Lazarov B. Topology optimization of unsteady flow problems using the lattice Boltzmann method. J Comput Phys 2016;307:291–307.
[11] Dirker J, Meyer JP. Topology optimization for an internal heat-conduction cooling scheme in a square domain for high heat flux applications. J Heat Transfer 2013;135(11).
[12] Zhang K, Li B, Du F, Liu H, Hong J. Topology optimization of natural convection heat transfer using SEMDOT algorithm based on the reduced-order model. Int Commun Heat Mass 2021;129:105676.
[13] Zhu J-H, Zhang W-H, Xia L. Topology optimization in aircraft and aerospace structures design. Arch Comput Method E 2016;23(4):595–622.
[14] Langelaar M. An additive manufacturing filter for topology optimization of print-ready designs. Struct Multidiscip O 2017;55(3):871–83.
[15] Haftka RT. Techniques for thermal sensitivity analysis. Int J Numer Meth Eng 1981;17(1):71–80.
[16] Meric RA. Boundary elements for static optimal heating of solids, Transactions of the ASME. J Heat Transfer 1984;106(4):876–80.
[17] Dems K. Sensitivity analysis in thermal problems—II: structure shape variation. J Therm Stresses 1987;10(1):1–16.
[18] Tortorelli DA, Haber RB, Lu SC. Design sensitivity analysis for nonlinear thermal systems. Comput Method Appl M 1989;77(1–2):61–77.
[19] Li Q, Steven GP, Xie YM, Querin OM. Evolutionary topology optimization for temperature reduction of heat conducting fields. Int J Heat Mass Tran 2004;47(23):5071–83.
[20] Li Q, Steven GP, Querin OM, Xie Y. Shape and topology design for heat conduction by evolutionary structural optimization. Int J Heat Mass Tran 1999;42(17):3361–71.
[21] Bendsoe MP, Sigmund O. Topology optimization: theory, methods, and applications. Springer Science & Business Media; 2003.
[22] Gersborg-Hansen A, Bendsøe MP, Sigmund O. Topology optimization of heat conduction problems using the finite volume method. Struct Multidiscip O 2006;31(4):251–9.

[23] Zhuang C, Xiong Z, Ding H. A level set method for topology optimization of heat conduction problem under multiple load cases. Comput Method Appl M 2007;196(4–6):1074–84.
[24] E.M. Dede, Multiphysics topology optimization of heat transfer and fluid flow systems, in: proceedings of the COMSOL Users Conference, 2009.
[25] Chen Y, Zhou S, Li Q. Multiobjective topology optimization for finite periodic structures. Comput Struct 2010;88(11–12):806–11.
[26] Burger FH, Dirker J, Meyer JP. Three-dimensional conductive heat transfer topology optimisation in a cubic domain for the volume-to-surface problem. Int J Heat Mass Tran 2013;67:214–24.
[27] K. Svanberg, H. Svard, Density filters for topology optimization based on the geometric and harmonic means, in: 10th world congress on structural and multidisciplinary optimization. Orlando, 2013.
[28] Sigmund O, Maute K. Topology optimization approaches. Struct Multidiscip O 2013;48(6):1031–55.
[29] Zhao Q, Fan C-M, Wang F, Qu W. Topology optimization of steady-state heat conduction structures using meshless generalized finite difference method. Eng Anal Bound Elem 2020;119:13–24.
[30] Lohan DJ, Dede EM, Allison JT. Topology optimization for heat conduction using generative design algorithms. Struct Multidiscip O 2017;55(3):1063–77.
[31] Liu T, Li B, Wang S, Gao L. Eigenvalue topology optimization of structures using a parameterized level set method. Struct Multidiscip O 2014;50(4):573–91.
[32] Díaaz AR, Kikuchi N. Solutions to shape and topology eigenvalue optimization problems using a homogenization method. Int J Numer Meth Eng 1992;35(7):1487–502.
[33] Tenek LH, Hagiwara I. Static and vibrational shape and topology optimization using homogenization and mathematical programming. Comput Method Appl M 1993;109(1–2):143–54.
[34] Ma Z-D, Kikuchi N, Hagiwara I. Structural topology and shape optimization for a frequency response problem. Comput Mech 1993;13(3):157–74.
[35] Ma Z-D, Kikuchi N, Cheng H-C. Topological design for vibrating structures. Comput Method Appl M 1995;121(1–4):259–80.
[36] Pedersen NL. Maximization of eigenvalues using topology optimization. Struct Multidiscip O 2000;20(1):2–11.
[37] Du J, Olhoff N. Topological design of freely vibrating continuum structures for maximum values of simple and multiple eigenfrequencies and frequency gaps. Struct Multidiscip O 2007;34(2):91–110.
[38] Achtziger W, Kočvara M. On the maximization of the fundamental eigenvalue in topology optimization. Struct Multidiscip O 2007;34(3):181–95.
[39] Ferrari F, Lazarov BS, Sigmund O. Eigenvalue topology optimization via efficient multilevel solution of the frequency response. Int J Numer Meth Eng 2018;115(7):872–92.
[40] Pereira DA, Sales TP, Rade DA. Multi-objective frequency and damping optimization of tow-steered composite laminates. Compos Struct 2021;256.
[41] de Kruijf N, Zhou S, Li Q, Mai Y-W. Topological design of structures and composite materials with multiobjectives. Int J Solids Struct 2007;44(22–23):7092–109.
[42] Marler RT, Arora JS. The weighted sum method for multi-objective optimization: new insights. Struct Multidiscip O 2010;41(6):853–62.
[43] He M, Zhang X, dos Santos Fernandez L, Molter A, Xia L, Shi T. Multi-material topology optimization of piezoelectric composite structures for energy harvesting. Compos Struct 2021;265:113783.
[44] Li D, Kim IY. Multi-material topology optimization for practical lightweight design. Struct Multidiscip O 2018;58(3):1081–94.
[45] Blasques JP. Multi-material topology optimization of laminated composite beams with eigenfrequency constraints. Compos Struct 2014;111:45–55.
[46] Habibian A, Sohouli A, Kefal A, Nadler B, Yildiz M, Suleman A. Multi-material topology optimization of structures with discontinuities using Peridynamics. Compos Struct 2021;258.
[47] Gao X, Chen W, Li Y, Chen G. Robust topology optimization of multi-material structures under load uncertainty using the alternating active-phase method. Compos Struct 2021;270.
[48] Banh TT, Luu NG, Lee D. A non-homogeneous multi-material topology optimization approach for functionally graded structures with cracks. Compos Struct 2021;273.
[49] Li Y, Xie YM. Evolutionary topology optimization for structures made of multiple materials with different properties in tension and compression. Compos Struct 2021;259.
[50] Giraldo-Londono O, Paulino GH. Fractional topology optimization of periodic multi-material viscoelastic microstructures with tailored energy dissipation. Comput Method Appl M 2020;372.
[51] Hassani B, Hinton E. A review of homogenization and topology optimization I - homogenization theory for media with periodic structure. Comput Struct 1998;69(6):707–17.
[52] Jie G, Hao L, Liang G, Mi X. Topological shape optimization of 3D micro-structured materials using energy-based homogenization method. Adv Eng Softw 2018;116:89–102.
[53] Guedes J, Kikuchi N. Preprocessing and postprocessing for materials based on the homogenization method with adaptive finite element methods. Comput Method Appl M 1990;83(2):143–98.
[54] Hassani B, Hinton E. Homogenization and structural topology optimization: theory, practice and software. Springer Science & Business Media; 2012.
[55] Andreassen E, Andreasen CS. How to determine composite material properties using numerical homogenization. Comp Mater Sci 2014;83:488–95.
[56] Xia L, Breitkopf P. Design of materials using topology optimization and energy-based homogenization approach in Matlab. Struct Multidiscip O 2015;52(6):1229–41.
[57] Sigmund O. Materials with prescribed constitutive parameters: an inverse homogenization problem. Int J Solids Struct 1994;31(17):2313–29.
[58] Bendsøe MP, Sigmund O. Material interpolation schemes in topology optimization. Arch Appl Mech 1999;69(9):635–54.
[59] Wang Y, Xu H, Pasini D. Multiscale isogeometric topology optimization for lattice materials. Comput Method Appl M 2017;316:568–85.
[60] M. Denk, K. Rother, K. Paetzold, Multi-Objective Topology Optimization of Heat Conduction and Linear Elastostatic using Weighted Global Criteria Method, in: Proceedings of the 31st Symposium Design for X (DFX2020), 2020.
[61] Giraldo-Londono O, Mirabella L, Dalloro L, Paulino GH. Multi-material thermomechanical topology optimization with applications to additive manufacturing: Design of main composite part and its support structure. Comput Method Appl M 2020;363.
[62] Zheng W, Wang Y, Zheng Y, Da D. Efficient topology optimization based on DOF reduction and convergence acceleration methods. Adv Eng Softw 2020;149:102890.
[63] Liao Z, Zhang Y, Wang Y, Li W. A triple acceleration method for topology optimization. Struct Multidiscip O 2019;60(2):727–44.
[64] Liao Z, Wang Y, Gao L, Wang Z-P. Deep-learning-based isogeometric inverse design for tetra-chiral auxetics. Compos Struct 2022;280:114808.